HHS Public Access

Author manuscript

Cancer Res. Author manuscript; available in PMC 2026 April 24.

Published in final edited form as:

Cancer Res. 2026 June 15; 86(12): 2878–2895. doi:10.1158/0008-5472.CAN-25-1527.

Ciliated Cells Drive Critical STING-Mediated Tumor Suppression in the Fallopian Tube Epithelium

Jose A. Colina[1,3], **Maria Sol Recouvreux**[11], **Alexander M Sobeck**[1,3], **Benjamin K. Johnson**[4], **Yinzhi Lin**[1,3], **Sreeja C. Sekhar**[1,3], **Rita A. Avelar**[1,3], **Gabriela Rivera**[1,3], **Yali Zhai**[1,3], **Harini Ram**[1,3], **Amber Fatima**[1,3], **Paula DiBenedetto**[1,3], **Justin Baldassarre**[1,3], **Grace McIntyre**[1,3], **Jessica Teitel**[1,3], **Michele L. Dziubinski**[1,3], **Noah Puleo**[1,3], **Jane Miglo**[5], **Karan Bedi**[6], **Hui Shen**[4], **Dafydd Thomas**[1], **Jutta Huvila**[7], **Dawn R. Cochrane**[8], **Ronny Drapkin**[9], **Yu L Lei**[10], **Joanna E. Burdette**[5], **Stephanie L. Skala**[1], **David G. Huntsman**[8], **Kathleen R. Cho**[1,3], **Sandra Orsulic**[11], **Analisa DiFeo**[1,2,3]

[1]Department of Pathology, University of Michigan, Ann Arbor, MI 48109, USA

[2]Department of Obstetrics and Gynecology, University of Michigan, Ann Arbor, MI 48109, USA

[3]Rogel Cancer Center, University of Michigan, Ann Arbor, MI 48109, USA

[4]Van Andel Research Institute

[5]University of Illinois Chicago

[6]Department of Biostatistics, University of Michigan, Ann Arbor, MI 48109, USA

[7]University of Turku

[8]British Columbia Cancer Research Centre

[9]University of Pennsylvania Perelman School of Medicine

[10]University of Texas MD Anderson Cancer Center

[11]University of California, Los Angeles

Abstract

Mitigating DNA damage in the fallopian tube epithelium (FTE) is essential for preventing tubo-ovarian high-grade serous carcinoma (HGSC). Here, we demonstrated that stimulator of interferon genes (STING) is abundantly expressed in the ciliated cells of the FTE and functions as a critical immune-independent tumor suppressor. In patient samples, mouse models, and organoid systems, ciliated cells mounted a dual protective response to ovulation-associated genotoxic stress: intrinsic STING-driven apoptosis and extrinsic clearance of neighboring damaged secretory cells via TNFα

Corresponding Author: Dr. Analisa DiFeo, adifeo@med.umich.edu, 1600 Huron Parkway , Ann Arbor, MI 48109.

AUTHOR CONTRIBUTIONS

Conceptualization, J.A.C and A.D.; Methodology, J.A.C and A.D.; Investigation, J.A.C., M.S.R., A.S., B.K.J., R.A., G.R., Y.Z., A.F., P.D., J.B., G.M., J.T., M.D., H.R., N.P., J.H., and D.C. ; Formal analysis, J.A.C., M.S.R. ,and A.S..; Software, J.A.C. and K.B.; Writing, J.A.C. and A.D., with input from all other authors; Visualization, J.A.C, R.A.; Funding Acquisition, J.A.C, A.D., R.D., K.C. and J.B.; Resources, J.M., H.S.,D.T., J.H., D.C., R.D. Y.L.L., J.E.B., S.S., D.H., K.R.C, S.O., and A.D.

CONFLICT OF INTEREST STATEMENT:

R.D. serves on the scientific advisory board of VOC Health and Repare Therapeutics. DGH is a previous founder and Chief Medical Officer of Imagia Canexia Health. The other authors declare that they have no competing interests.

secretion. This surveillance mechanism markedly limited DNA damage accumulation within the epithelial microenvironment. Crucially, while these mechanisms were vital for maintaining homeostasis and reducing genomic instability, they failed to impact p53-deficient precursor lesions as both the intrinsic and extrinsic pro-apoptotic processes relied on functional p53 signaling. These findings redefine ciliated cells as key gatekeepers of genome integrity rather than passive bystanders and implicate early loss of STING-high ciliated cells as a pivotal event in HGSC initiation.

Introduction

Ovarian cancer is the sixth leading cause of cancer deaths among women[1]. Tubo-ovarian high grade serous ovarian carcinoma (HGSC), which constitutes more than 70% of epithelial "ovarian" cancers, accounts for the majority of these mortalities[2]. Less than 10% of HGSC diagnoses are made at stage I and thus 5-year survival rates remain low.[2] In order to devise innovative prevention and treatment strategies a better understanding of early disease trajectory is needed. HGSC most commonly originates from precursor lesions arising in secretory cells of the fallopian tube epithelium (FTE) in the tubal fimbriae and is marked by *TP53* mutations leading to a high degree of genomic instability, yet the mechanisms that safeguard genomic stability in this tissue remain poorly defined.[2–7]. Ovulation is a key driver of early HGSC development by acting as a repeated and acute genomic stressor[8–11]. Reactive oxygen species, inflammatory mediators, glycation end products, hormones, and other substances present in follicular fluid bathe the fimbriated end of the fallopian tube during ovulation, thereby inducing DNA damage and inflammation[9,10,12–16] Recent findings have also shown that p53 loss enhances the transcription of immunogenic repetitive elements, triggering chronic viral mimicry activation. This persistent activation induces cellular tolerance to cytosolic nucleic acids, promotes genomic instability, and progressively diminishes immunogenicity, ultimately driving cancer progression[17].

The ability of the FTE to abrogate this compounding genomic instability is critical to avoid transformation. HGSC is associated with advanced age with the majority of patients diagnosed at age 50 or older[18–20]. Therefore, recent efforts have been focused on better understanding what physiological changes associated with age may contribute to carcinogenesis. A handful of studies have identified pro-tumorigenic shifts in the composition of follicular fluid of older women particularly noting that it is more rich in reactive oxygen species and causes more DNA damage than follicular fluid of younger women[12,21]. This increasingly genotoxic milieu released during ovulation is further accompanied by a notable decline in the population of ciliated cells within the fallopian tube with age[22]. It has been demonstrated that a reduction in the number of ciliated cells in the FTE is associated with an increased risk of developing HGSC even when controlled for age[22,23]. While ciliated cells are not considered the cell of origin for HGSC, it has been shown that the presence of ciliated cells decrease with HGSC progression[22,24–26] suggesting, they may be playing an underappreciated role in maintaining genomic integrity in the FTE. Indeed, ciliated cells have emerged as key modulators in the development of other malignancies, including pancreatic cancer, basal cell carcinoma, and medulloblastoma[27–29].

Most recently it has been shown that ciliated cells in the FTE are rich in STING (Stimulator of Interferon Genes), a key mediator in cellular the response to DNA damage[30,31]. The STING signaling axis is an evolutionarily conserved pathway essential for the detection of infection-derived nucleic acids as well as DNA damage induced cytosolic DNA, facilitating the initiation of innate immune responses necessary for host defense[32–34]. This pathway has also been well studied for its tumor suppressive functions in coordinating anti-tumor immunosurveillance[34–37]. Further, there is increasing evidence that the STING pathway plays an immune-independent role in suppressing tumorigenesis by reducing genomic instability both intrinsically and extrinsically[36,38–40]. Ectopic cytosolic DNA, often occurring during infection or acute DNA damage, is enzymatically converted to cGAMP by cGAS which acts as a STING ligand. Upon activation, STING oligomerizes and translocates from the ER to the Golgi where it then recruits TANK Binding Kinase1 (TBK1) which in turn phosphorylates STING, IRF3, NF-KB, and trans-autophosphorylates further TBK1 kinases [33,41,42]. This cascade ultimately leads to the secretion of type I interferons and inflammatory cytokines. Importantly, signaling strength-dependent activation of this pathway can trigger cell cycle arrest, senescence, intrinsic programmed cell death and secretion of a pro-apoptotic paracrine signals[40,43–46]. These mechanisms are crucial to the pathway's ability to resolve sterile tissue damage through the arrest or elimination of genomically unstable cells. Furthermore, we have previously shown that STING loss drives transformative phenotypes in pre-malignant fallopian tube secretory cells by allowing the persistence of genomically unstable cells[47]. In this current study we demonstrate that STING-high ciliated cells in the FTE detect cytosolic DNA generated by ovulation-associated oxidative stress and initiate caspase-dependent apoptosis to eliminate damaged neighboring secretory cells.

Furthermore, by analyzing four independent patient cohorts encompassing precursor lesions, early-stage HGSC, and advanced disease, we demonstrate that STING loss is an early and consistent event in tumorigenesis, coinciding with the decline of ciliated cells observed in both mouse models and oviductal organoids. These findings highlight a previously unrecognized function of ciliated cells in safeguarding epithelial homeostasis through STING-driven intrinsic apoptosis and extrinsic clearance of genomically unstable secretory cells. Crucially, we identify a novel p53 dependency that underlies the anti-tumorigenic activity of STING, revealing a critical barrier to malignant progression that is lost with p53 dysfunction.

Methods

Immunofluorescent imaging of HGSC TMA

Multiplex immunofluorescence staining was performed by the UCLA Translational Pathology Core Laboratory using The Opal Polaris 7-Color Automation Kit (Akoya Biosciences, Cat# NEL871001KT) as previously described[24] in addition to 4′,6-diamidino-2-phenylindole (DAPI, Akoya Biosciences CAT# SKU FP1490) and primary antibodies against STING (TMEM173, Atlas Antibodies Cat# HPA038116, 1:100 dilution), calcyphosine (CAPS, Atlas Antibodies Cat# HPA043520, 1:1000 dilution), and Acetylated

Tubulin (Anti-Acetylated Tubulin mouse IgG2b isotype, Sigma Aldrich Cat# T7451, 1:1000 dilution)

Low stage HGSC TMA immunohistochemical analysis

This study was performed on a TMA with 0.6 mm cores from FFPE tissues comprised of 30 cases, including cores from healthy fallopian tube, fallopian tube from patients with gynecological inflammation resulting from endometriosis or chronic salpingitis, and Stage I/Stage II HGSC obtained from Tissuearray.com (cat# UTE601). We stained the TMA for STING (Cell Signaling cat#13647) and P53 (DAKO M7001) (Supplementary Table S1) samples were scored by a practicing surgical pathologist (SS).

Case selection of precancerous lesions

The cases for this study were obtained from the Departments of Pathology at Brigham and Women's Hospital and the Hospital of the University of Pennsylvania. Formalin-fixed paraffin embedded (FFPE) blocks of fallopian tube tissues were cut from 8 cases whose original pathology reports indicated the presence of HGSC in addition to a diagnosis of STIC and benign FT epithelium. We also obtained 17 cases from Department of Pathology at Michigan Medicine of from patients who were diagnosed with HGSC and had the presence of p53 signature or STIC lesions. Lastly, we obtained 17 cases from the British Columbia Cancer Research Centre. Participants provided written informed consent to either Michigan Medicine, Brigham and Women's Hospital, University of Pennsylvania, or British Columbia Cancer Research Centre IRB-approved protocols. These hematoxylin and eosin (H&E) slides were reviewed by three pathologists (SS, KC, RD) to confirm the presence of STICs and possibly invasive carcinoma in the deeper tissue sections. All patient studies were conducted in accordance with Declaration of Helsinki, International Ethical Guidelines for Biomedical Research Involving Human Subjects (CIOMS), Belmont Report, U.S. Common Rule.

Re-analysis of publicly available human fallopian tube scRNA-seq data

Primary human fallopian tube (FT) scRNA-seq were downloaded from the following repositories: 1) FTE STORM-seq transcript abundance counts (TPM) GSE296406, 2) SMART-seq2 raw FASTQs GSE139079, 3) Ulrich et al[48].10x Genomics h5ad object from the CZI Cell Science Cell x Gene (https://cellxgene.cziscience.com/collections/fc77d2ae-247d-44d7-aa24-3f4859254c2c), 4) Weigert et al[49]. 10x Genomics h5ad object from the CZI Cell Science Cell x Gene (https://cellxgene.cziscience.com/collections/380ade76-e561-49a8-afb2-0f10b39c2c72). STORM-seq and SMART-seq2 data were mapped and processed as previously described (Biorxiv 2022.03.14.484332v4). Briefly, for STORM-seq and SMART-seq2, raw TPM values were adjusted for duplication rate using the izar_transform() function within velocessor (v0.15.27) and R (v4.4.1), as previously described[50]. Principal component analysis (PCA) was performed using the runPCA function in scater (v1.16.0), retaining 20 components using the top 10% most variable genes. Cluster analysis was performed using the retained PCs and building a shared nearest neighbor graph with the buildSNNGraph() function in scater, then clusters were identified using the cluster_walktrap function in igraph (v1.2.6). Cluster annotation was performed for STORM-seq and SMART-seq2 using known marker genes and cell identity ontologies within the

human fallopian tube (https://www.ebi.ac.uk/ols4/). The 10x Genomics h5ad objects were converted to SingleCellExperiment objects using zellkonverter (v1.14.1). 10x Genomics datasets were annotated using the author provided cluster annotations. The Weigert et al. data were subset to the fimbriated end of the fallopian tube. For STING1 expression visualization in secretory and ciliated cells, other cell types were masked prior to plotting expression for consistency with other comparisons within this work. Plots were generated using ggplot2 (v3.5.1). Statistical tests between STING1 expression in ciliated cells and other cell identities were done using ggpubr (v0.6.0). Briefly, pairwise Wilcoxon Rank Sum tests were conducted with Benjamin-Hochberg FDR correction, and significance was determined by setting an adjusted $p < 0.05$.

Single cell RNAseq analysis of patient fallopian tubes

Fallopian tubes from 10 patients were collected by the UCLA Pathology team, placed in DMEM media, and transferred in ice to the lab for further processing. Preparation for single-cell RNA sequencing was done as previously described[51]. Partek flow software was used for thresholding and single-cell RNA sequencing data analysis. Cells were removed according to the following criteria: 1) cells had fewer than 500 genes or more than 10000 genes; 2) cells had fewer than 500 unique molecular identifiers (UMI) or over 10000 UMI; and 3) cells had more than 10% of mitochondrial UMI counts. For cell identification we used the following markers: Epithelial cells: EPCAM, KRT18, PAX8, FOXJ1; Fibroblast: PDGFRA, COL1A1; T and NK cells: CD8A, CD3E, NKG7; Macrophages: CQ1, CD68; Mast cells: TPSAB1; Endothelial Cells: CLDN5, CDH5; B Cells: JCHAIN, CD79A; Neutrophils: S1008A, S100A9. Epithelial cells were re-clustered to identify ciliated and secretory cell clusters.

Isolation from patient fallopian tube epithelial cells

Fallopian tubes from normal (non-cancer) patients were collected by TPCL core (UCLA) and stored in fresh DMEM media at 4°C until delivered to the lab. Ampullas are first cleaned from connective tissue, opened in half to expose the epithelium, and chopped into small pieces ~1mm. Tissue is then further dissociated by enzymatic digestion by rotating at 37°C for 45 minutes with 1 mg/ml Collagenase/Hyaluronidase (STEMCELL Cat #07912), DNAse (100units), trypsin (0.01%), and 2% FBS on DMEM media. After dissociation, the suspension is strained (70 μm) followed by centrifugation (8 minutes at 300 g). Red blood cells are removed using red blood cell lysis buffer (Thermo Fisher Cat # 00–4333-57). The resultant cells are plated in pre-coated with Matrigel (Corning) 12 well plates or 8-chamber slides in special media: advanced Dulbecco's modified Eagle medium/F12 supplemented with 12 mmol/L HEPES, 1X Glutamax, 2% B27, 1% N2 (all from Life Technologies), 10 ng/mL murine recombinant EGF (Peprotech Cat # 315–09-500UG), 10 ng/mL basic FGF(Peprotech Cat # 100–18B-50UG), 30 ng/ml human Noggin (R&D systems Cat # 6057-NG-025), 0.5 mM TGF-b R Kinase Inhibitor IV (Sigma-Aldrich Cat #616461) and 1% penicillin/ streptomycin (Invitrogen Cat #15140122) and freshly added: 10 μM ROCK inhibitor Y-27632 (Selleckchem Cat # S1049), wnt3a 100ng/ml (R&D systems Cat #5036-WN), β-estradiol 10nM. Secretory-only cultures were achieved by passaging the primary cultures using trypsin for 5–7 minutes. To inhibit STING, H-151 (Tocris Cat# 6675) was used at 1μM.

STING correlation with FOXJ1 and PAX8 in normal FT and HGSOC

Bulk RNA sequencing data from normal fallopian tube samples from 59 women (unpublished data from the Dr. Sandra Orsulic) and 541 HGSC (TCGA) were analyzed. Pearson correlation analysis was done using Graph pad Prism 7.

Animals

All animal studies were performed according to protocols approved by the University of Michigan's Institutional Animal Care and Use Committee (IACUC). Female C57BL/6J mice (Jackson Laboratory, Cat #000664) were purchased from Jackson Laboratory and C57BL/6J-STING1gt/J mice (Jackson Laboratory, Cat #017537) were gifted to our lab from Yu Leo Lei, at MD Anderson Cancer Center, University of Texas.

Ovarian Stimulation for Superovulation

5 to 7 week-old mice were superovulated using a well-established protocol from the Jackson Laboratory. Briefly, female mice are injected interperitoneally (IP) with 5U of pregnant mare serum gonadotropin (PMSG) (Fisher Scientific, Cat #50–168-5796) between 1–4pm on Day 1. 48 hours later, on Day 3, mice were injected with 5U of human chorionic gonadotropin (hCG) (Sigma, Cat #C1063) interperitoneally. The mice oviducts were harvested from mice on Day 4, 12–24 hours post hCG injection.

Immunohistochemical Analysis of Mouse Reproductive Tracts

Mouse reproductive tract tissues were fixed in 4% of formaldehyde for 48 hr, and paraffin-embedded through the Tissue and Molecular Pathology core at the University of Michigan. Immunohistochemistry analysis of murine reproductive tracts was performed on a DAKO autostainer. Slides were subjected to epitope retrieval using 10 mM Tris–HCl buffer pH 9.0 containing 1 mM EDTA. The slides were then subjected to H_2O_2 and protein exposure to remove non-specific binding. The slides were exposed overnight to primary antibody (Supplementary table S2) after washing with TBST. The slides were exposed to DAKO Envision+ (Goat antimouse polymerized HRP) and subsequently the chromogen, diaminobenzidine (DAB). After counterstaining with hematoxylin, the slides were digitally scanned using an APERIO scanner. In order to determine the specificity of the antibody, the antibody was pre-incubated with 10x molar excess of the methylated and unmodified peptides prior to incubation with slides.

Multiplex immunofluorescence analysis of murine reproductive tracts was conducted after optimization of the staining parameters for each individual primary antibody, the slides were sequentially stained with the following antibodies (CD69 (Opal 620), CD163 (Opal 690), CD8a (Opal 570), CD4 (Opal 480), NCR1 (Opal 520) and CD3 (Opal 780) using a Ventana Discovery Ultra stainer. After the primary antibody incubation, the slide was washed with TBST and Ventana Omnimap anti-rabbit HRP was applied. The application of Opal Tyramide Signal Amplification (TSA); as detailed above; thus creating a covalent bond between the fluorophore and the tissue at the HRP site. Subsequent heat induced epitope retrieval using CC2 buffer removed the primary antibody/secondary antibody complex, and the next antibody was applied. Thus, a panel of 6 fluorochromes was sequentially applied to the tissue. The slides were then mounted with Prolong gold containing DAPI and scanned

using an Akoya Polaris IF scanner at x20 magnification. The digital slides were examined and quantified QuPath(Version 0.4.3). Images were analyzed to determine staining intensity on a per-cell basis, with automated scoring based on chromogenic signal intensity. Cells were manually classified into +1, +2, or +3 categories using an intensity threshold. Any cell scoring +1 or higher was considered positive, and positivity was expressed as the percentage of total cells counted.

Western Blot Analysis

Total protein lysates were prepared from cell pellets using RIPA buffer supplemented with an EDTA-free Protease and Phosphatase Inhibitor Tablet (ThermoScientific Cat# A32961). Total protein lysates from murine oviductal organoids or animal tissue required an additional extraction step before lysis. Organoid material was separated from extracellular matrix using Cultrex Organoid Harvesting Solution (R and D systems Cat# 3700–100-01) following the manufacturer's protocol. Organoids were then centrifuged and the cell pellets lysed with RIPA. Murine tissue was digested using a Tumor Dissociation Kit (Miltenyi Biotec, Gladbach, Germany) according to the manufacturer's instructions. Briefly, the tissue sample was minced, and the pieces were transferred to a gentle MACS C Tube containing RIPA. The gentle MACS™ Dissociator was used for the mechanical dissociation step followed by centrifugation. Protein concentration was determined using the BCA assay and read on the BioTek Cytation 5 microplate reader. Western Blots were run as described previously. All primary and secondary antibodies used are detailed in Supplementary table S3.

Organoid Culture

Organoids were derived from the oviducts of C57BL/6 mice using methods shown previously[52]. Oviducts were dissected, finely minced, then digested for 2hr at 37 °C in collagenase/ hyaluronidase (1mg/mL)(STEMCELL Cat #07912), 1X Glutamax (Fischer Scientific Cat # 35050061), 10mM HEPES, 1% Penn strep, and 10uM ROCKi (Selleckchem Cat # S1049). Cells were then washed and dissociated using TRYPLE (Thermo Fisher Cat # 12605036) for 5min at 37 °C followed by mechanical dissociation by repeated pipetting. Cells were then washed and pelleted before being mixed with RGF Basement Membrane Extract, Type 2 (RandD systems Cat # 3533–010-02) and subsequently plated into 12-well suspension culture plates(Greiner Bio-One Cat #665102). Organoids were cultured in a 50/50 mix of Advanced DMEM-F12 (Gibco 12–634-010) and LWRN conditioned media supplemented with 1% N2 growth supplement (ThermoFisher Cat #17502001), 2% B27 growth supplement (ThermoFisher Cat #17504044), 50 ng/mL EGF (ThermoFisher Cat # PMG8043), 100 ng/mL FGF (Peprotech Cat # 100–18B-50UG), 9uM ROCKi Y27362 (Selleckchem Cat # S1049), 10nM Estradiol , 500nM TGFBi A-83 (Selleckchem Cat # S7692). To make LWRN media The LWRN cells (ATCC Cat # CRL-3276) were cultured in Advanced DMEM-F12 with 20% FBS (v/v) (Denville Scientific) supplemented with 1% Glutamax (Fischer Scientific Cat #35050061) and 1% penicillin/ streptomycin (v/v) (Invitrogen Cat #15140122) for 24 hours. Media was then harvested, filtered, and stored at −80 °C.

p53−/− organoids were derived from the oviducts of *Ovgp1-iCreER^{T2}* mice. *Ovgp1-iCreER^{T2}* mice in which the Ovgp1 promoter controls expression of tamoxifen (TAM)-

regulated Cre recombinase in oviductal epithelium, were developed by the University of Michigan Transgenic Animal Model Core and have been described previously[53]. *Ovgp1-iCreER^{T2}* transgenic mice were crossed with mice carrying engineered floxed *Trp53* alleles, to generate transgenic mice in which Cre-mediated recombination generates null alleles[54]. One passage after organoid culture establishment these organoids were treated with 1μg/mL 4-Hydroxytamoxifen (Sigma-Aldrich #H6278) over 7 days, with media being changed and the treatment being reapplied every 2 days. Knockout was confirmed by western blot.

RNA Extraction and qRT-PCR

mRNA from patient derived fallopian tube epithelial cells and murine oviductal epithelial cells were isolated using RNeasy Plus Mini Kits (Qiagen Cat# 74134). mRNA from murine oviductal organoids were isolated using miRNeasy Mini Kits (Qiagen Cat# 217004). To determine mRNA expression levels, 1000 ng of total RNA was reverse transcribed into cDNA using the High-Capacity RNA-to-cDNA™ Kit (ThermoScientific Cat# 4387406). cDNA was then PCR amplified using a QuantStudio 5 Real-Time PCR machine along with gene-specific PCR primers and PowerTrack™ SYBR Green Master Mix (ThermoScientific Cat# A46111). Primers used are listed in supplementary table S4.

Differential Gene expression and Gene Set Enrichment Analysis of Follicular Fluid Treatment of Oviductal Organoids

Organoids were generated from mouse oviductal epithelium from wild type B6 mice aged 8–12 weeks. organoids were exposed to human follicular fluid at a 1:1 ratio with organoid media[12,13,55]. Because follicular fluid is initially released in high concentrations at the fimbrial end before undergoing dilution in the peritoneal cavity, our use of 50% FF likely represents a conservative approximation of the acute exposure experienced by fallopian tube epithelial cells immediately post-ovulation. Follicular fluid was gathered from patients from Michigan Medicine (IRBMED # HUM0133335) under IRB consented protocol. Organoids were harvested after 24 hours of exposure to follicular fluid or PBS. Four replicates were used for extraction of RNA for analysis by RNA-seq. Gene set enrichment analyses (GSEA) were performed comparing follicular fluid treatments back to PBS control[56]. Differentially expressed genes were compared against the “Hallmark” database. Gene sets with an p-value of less than 0.05 were considered significant.

Cell Culture

Murine oviductal epithelial (MOE) cells were obtained from Dr. Joanna Burdette (University of Illinois at Chicago) and were generated as previously described[57]. Cells were cultured in α-MEM (Corning Cat # 10–022-CV) supplemented with 10% v/v fetal bovine serum (FBS; Gemini #100–106), 2 mM L-glutamine (Gibco #25030081), 2 μg/ml epithelial growth factor (Peprotech #AF-100–15), 1 mg/ml gentamycin (Corning #30–005-CR), 50 U penicillin, 50 μg/ml streptomycin and 18.2 ng/ml β-estradiol. All cell lines were authenticated via STR profiling and confirmed negative for mycoplasma testing, completed quarterly.

For conditioned media experiments, donor cells (MOE:SCR or MOE:SO) were challenged with 500μM H_2O_2 for 24hr. Conditioned media was then collected and filter through a .22 micron filter. For TNFi experiments, conditioned media was incubated with a neutralizing

antibody against TNFα (Cells Signaling Cat# 11969) for 1hr. Conditioned media was then put onto recipient cells and additional H_2O_2 was added.

Lentiviral Transduction

Lentiviral particles were generated in HEK 293T cells using vectors from supplementary table S5 in co-transfection with psPAX2 and pMD2.G as packaging and envelope, respectively. Virus containing media was collected on day 2 and 3, filtered, and supplemented with 8 μg/ml polybrene before added to the MOE parental target cells for 24 hours. At day 4, viral media was replaced with normal media and 24 hours later, 16 μg/ml of Blasticidin was added for 1 week to select positively transfected cells. 8 μg/ml of Blasticidin was used then forward as a maintenance dose. Western blotting was used to confirm overexpression.

Immunofluorescence Staining

Immunofluorescent analysis of murine cells was conducted as previously described[58]. Cells were plated on glass cover slides precoated with Poly-D-Lysine (Thermo Fisher Cat # A3890401). Cells were fixed with paraformaldehyde for 10 minutes at room temperature and permeabilized with a 0.25% Triton X-100 solution. Cells were then blocked with 1% BSA in PBST. Primary antibodies γH2AX (abcam Cat# ab26350, 1:1000) and Rad51 (abcam Cat# ab133534, 1:1000) were incubated with cells overnight followed by secondary antibody staining for 1hr and room temperature. Cells were then incubated with a conjugated primary antibody against STING (Cell Signaling Cat# 90173). After staining, the cells were mounted on microscope slides with mounting solution containing DAPI (Thermo Fisher Cat# P36931) and imaged using a Leica DMI6000 inverted microscope. Images were analyzed using imageJ. For co-culture experiments MOE:SCR cells were cultured either alone or at a 1:1 ratio with MOE:SO cells with equal numbers of total cells in each well. For analysis of co-cultured MOE:SCR and MOE:SO samples, γH2AX foci per nucleus were automatically quantified using ImageJ, and the data were then manually classified as MOE:SO or MOE:SCR based on perinuclear STING expression.

Colony Formation Assay

Cells were plated in 12-well plates at a density of 500 cells/well and challenged with peroxide. After 7 days, cells were fixed with 10% methanol, 10% acetic acid (v/v) in dH2O for 1hr. After fixing, the cells were stained with 5% (w/v) crystal violet in 100% methanol overnight. Plates were then imaged and colonies in each well were quantified using ImageJ software.

Cell Viability

Cell viability was assessed via sulforhodamine B (SRB) assay. Cells were seeded in 96-well clear, flat-bottom plates at a density of 1,000 cells per well and treated with peroxide. Cells were then incubated at 37 °C for 5 days before being fixed and stained with sulforhodamine B (Fisher Scientific Cat # A060025G). Cells were then analyzed using colorimetric absorbance at 505 nM on a BioTek Cytation 5 microplate reader.

In vitro Apoptosis Assay

To assess apoptosis *in vitro,* cells were seeded in 96-well white-walled flat-bottom plates at a density of 1,000 cells per well and treated with peroxide. Accumulation of apoptotic cells was quantified with RealTime-Glo Annexin V Apoptosis and Necrosis Assay (Promega Cat # JA1011) according to the manufacturer's protocol.

Annexin V/PI Flow Cytometry

GFP-tagged MOE:WT cells were cultured alone or co-cultured at a 1:1 ratio with MOE STING-OE cells. Co-cultures were then treated with peroxide for 24 or 48 hours. Trypsinized cells were collected and centrifuged at 300 × g at 4 °C for 5 minutes, washed once with PBS, and centrifuged again. Cell pellets were resuspended in 1× Annexin V Binding Buffer (Invitrogen Cat# V13246) with Annexin V Pacific Blue (ThermoScientific Cat# A35122) followed by propidium iodide (ThermoScientific Cat# V13241B), according to the manufacturer's instructions. Flow cytometry was performed using a Bigfoot Spectral Cell Sorter, and GFP-positive cells were gated to exclude MOE STING-OE cells. Apoptosis was quantified in the GFP-positive (STING-Low MOE:WT) population using FlowJo.

Resource Identification

Research Resource Identifiers (RRIDs) for all antibodies, experimental models, recombinant DNA, software, and other key resources used in this study are provided (Supplementary Table S6).

Data Availability Statement

The RNAseq data analyzed in this are available in the Gene Expression Omnibus under accession code GSE308878. Previously published RNA sequencing data that were reanalyzed here are available in the Gene Expression Omnibus under accession code GSE296406(Biorxiv 2022.03.14.484332v4) and GSE139079[59]. All other raw data are available upon request from the corresponding author.

Results

STING loss is an early and prevalent feature in HGSC development

Given the high STING expression in normal fallopian tube epithelium (FTE), we examined STING levels across healthy FTE and various HGSC stages[30,31]. In all healthy samples, STING was strongly expressed in ciliated cells throughout the epithelium (Figure 1A). In contrast, most HGSC tumors showed absent or markedly reduced STING expression (Figure 1A; Supplementary Figure 1A, Supplementary Table S7). Notably, in advanced (stage III/IV) tumors with residual STING expression, STING did not co-localize with ciliated cells (Supplementary Figures 1B, 1C). Supporting these findings, bulk RNA sequencing of 59 normal FTE samples and 541 HGSC cases (TCGA) revealed a strong positive correlation between FOXJ1 (a ciliated cell marker) and STING in normal tissue (R=0.75, p=1.35×10^−11), but not in HGSC (R=0.03, p=0.43). There was no significant association between STING and PAX8, a secretory cell marker, in either FTE or HGSC (Supplementary Figure 1D).

To further validate these findings, we examined STING expression in an additional cohort of healthy, inflamed, and early-stage precursor fallopian tube (FT) lesions (Figure 1B; Supplementary Figure 1E–F, Supplementary Table S8). Consistent with our initial analyses, we observed robust STING expression predominantly in ciliated cells of normal FT epithelium. Inflamed samples showed a similar pattern, with STING expression largely confined to ciliated cells. In contrast, stage I and II HGSC samples were devoid of detectable STING expression (Figure 1B). To better define changes in STING expression during neoplastic progression, we analyzed a third cohort including invasive HGSC, serous tubal intraepithelial carcinomas/lesions (STICs/STILs), and p53 signature lesions from 42 patients. Given that STIC lesions and HGSC are primarily composed of secretory cells, which express little if any STING, STING expression was found to be low or absent in 97.1% of precancerous lesions (Figure 1C). Notably, loss of STING closely paralleled the decline of ciliated cells and inversely correlated with mutant p53 accumulation, providing a clear molecular boundary for early lesion development. This pattern reflects the overall reduction of STING-positive ciliated cells as the tissue transitions from healthy epithelium to early neoplastic states.

To further examine the clinical relevance of our findings and investigate whether STING is predominantly expressed in ciliated cells, we analyzed single-cell RNA sequencing (scRNA-seq) data from normal FTE of five premenopausal patients undergoing benign salpingectomies (Figure 1D, Supplementary Figure 2A). STING expression was significantly higher in differentiated ciliated cells than in other epithelial populations, including secretory cells, intermediate branch point cells, and unclassified progenitors ($p < 0.01$, Figure 1D). These findings were validated in 10 additional patient samples, confirming enriched STING expression in ciliated versus secretory epithelial cells (Supplementary Figure 3A–E). Consistent results were observed in published scRNA-seq datasets from Ulrich et al. and Weigert et al., showing STING enrichment in ciliated cells relative to other epithelial and immune cell types in the fallopian tube (Figure 1E)[48,49].

These data indicate that loss of ciliated cells depletes STING expression in the FTE microenvironment, and this is an early and prevalent feature in the development of HGSC. Importantly, since epithelial precancerous lesions of the fallopian tube are defined as outgrowths of secretory cells, this may contribute to our finding that STING is absent in even early precancerous lesions. However, it remains unclear if this compounding loss of STING in the microenvironment could predispose the FTE to HGSC development.

The cGAS-STING pathway senses cytosolic DNA to respond to genomic instability. In the fallopian tube, ovulation exposes the fimbriated end to hormones, cytokines, and reactive oxygen species that induce acute DNA damage, [8,9,12–14,17]. To better understand if loss of STING-high ciliated cells impairs the tissue's ability to respond to genomic stress, we challenged patient-derived primary FTE cells with reactive oxygen species (ROS). Primary FTE collected from patients undergoing salpingectomies for benign indications were cultured and either retained as ciliated-secretory cell mixed populations (Cilia-High) or passaged to create a secretory cell-only population (Cilia-Low) (Supplementary Figure 3F); these were then challenged with ROS-inducing hydrogen peroxide (H_2O_2) as a mimetic of follicular fluid-induced genomic stress brought on by ovulation. The ciliated-secretory

cell mixed populations had significantly reduced accumulation of γH2AX compared to their secretory-only counterparts (Figure 1F). Furthermore, the presence of STING-high ciliated cells in the microenvironment significantly reduced the accumulation of H2AX positive secretory cells when exposed to H_2O_2 (Supplementary figure 3G). Additionally, only the cilia-high group responded to the ROS by inducing transcription of STING pathway target genes *IFNB1* and *CXCL10* (Supplementary Figure 3H). To confirm that activation of STING was contributing to this reduced γH2AX accumulation, we co-treated the populations with the covalent STING inhibitor H-151. We observed a significant increase in γH2AX accumulation in the cilia-high population treated with H-151 compared to H_2O_2 alone (Figure 1F, p=0.0310). Importantly, blocking STING in the mixed populations promoted the accumulation of γH2AX positive secretory cells (Supplementary figure 3G). These data taken together suggest that STING's function in the microenvironment contributes to reducing DNA damage accumulation.

Loss of STING in the oviducts leads to an accumulation of DNA damage

Genomic damage caused by acute ovulatory stress in the fallopian tube is a key driver of HGSC development; thus, the FTE's ability to manage this stress is critical to avoiding transformation. It has been hypothesized that ciliated cells may provide the FTE relief from genotoxic stress through physical clearance of follicular fluid through ciliary beating [22,24–26] However, since we observed that the STING pathway is induced in cilia-high FTE populations upon ROS exposure and that blocking STING with a small molecule inhibitor increased the accumulation of γH2AX we hypothesized that loss of STING alone, while maintaining the ciliated cell population, would be sufficient to increase post-ovulatory DNA damage accumulation in the fallopian tubes. To test this, we examined the effect of superovulation on STING deficient (*STING−/−*) and wild type (WT) mice, as superovulation is known to induce DNA damage in the mouse oviducts[10]. Despite our evidence that STING is strongly associated with ciliated cell differentiation, STING loss did not affect the number of ciliated cells in the FTE as shown by the expression of acetylated tubulin (Figure 2A&B). As expected, *STING−/−* oviducts exhibited markedly less phospho-TBK, the direct downstream marker of STING activation, post-superovulation compared to control; the presence of limited phospho-TBK expression in these samples suggests some degree of STING-independent TBK activation. In contrast, WT oviducts displayed robust phospho-TBK expression post-ovulation in cells interspersed throughout the epithelium confirming that ovulatory stress induces the STING pathway(Supplementary figure 4A & 4B). We also observed high STING expression in the WT murine uterus; however, post-ovulation the endometrial epithelium did not strongly express Phospho-TBK suggesting that the pathway is not induced in this tissue (Supplementary figure 4A & 4B). Like the results observed in our human primary FTE patient samples, γH2AX accumulation was significantly higher in STING-deficient mice compared to WT after superovulation (Figure 2B). Activation of the cGAS-STING pathway has been shown to limit DNA damage accumulation by inducing both intrinsic and extrinsic programmed cell death[36,38–40]. Consistently, we observed significantly higher TUNEL staining in WT oviducts, whereas STING knockout oviducts from superovulated mice exhibited reduced TUNEL positivity (Figure 2B), suggesting that STING deficiency allows cells to evade apoptosis and accumulate genomic instability.

STING activation has been well studied for its role in facilitating anti-neoplastic immune surveillance through type I interferon mediated stimulation of immune infiltration and activation. Despite this, STING loss did not significantly impact the immune microenvironment of the reproductive tract post-ovulation (Figure 2C). Neither super-ovulated WT mice, nor *STING−/−* mice experienced a significant change in total CD45+ immune cells (Figure 2C). There was also no significant change in the accumulation of macrophages (F40/80+), NK cells (NCR1+), or T Cells (CD3+) (Figure 2C & 2D). Utilizing multiplex IHC we also explored the possibility that the reproductive tracts of WT mice may be enriched for CD8+ cytotoxic T cells and that loss of STING might inhibit their accumulation. No significant shift in T cell subpopulations post-ovulation nor a significant change in these populations in the reproductive tracts of *STING−/−* mice were observed (Figure 2D). Lastly, we aimed to exclude the possibility that the reduction in γH2AX accumulation observed in WT oviducts compared to *STING−/−* is a result of the adaptive immune cell clearance of genomically unstable cells post-ovulation. To achieve this, we subjected *RAG1−/−* mice, which are devoid of B or T cells, to super-ovulation and observed no significant difference in γH2AX or TUNEL accumulation compared to WT mice (Figure 2E) (Supplementary figure 4C). These data demonstrate that loss of STING in the reproductive tract does not significantly alter the acute immune response to ovulation suggesting that the differential DNA damage response observed in STING-deficient mice is immune independent.

Given that immune cells did not account for the reduced γH2AX accumulation in STING-competent mice after superovulation, we generated oviductal organoids from STING−/− and WT mice to investigate epithelial-intrinsic mechanisms of STING-mediated DNA damage mitigation. Both organoid types retained secretory and ciliated cell populations (Figure 3A–B, Supplementary Videos 1–2). Organoids were challenged with 500 μM H_2O_2 to mimic acute ovulatory ROS stress, consistent with human follicular fluid ROS levels[14]. WT organoids activated the STING pathway, inducing TBK phosphorylation, whereas STING−/− organoids failed to do so (Figure 3C). STING deficiency resulted in greater γH2AX accumulation, reduced p53 and p21 induction, and impaired upregulation of p53 target genes CDKN1A, GADD45A, and MDM2 in response to ROS (Figure 3C–D, Supplementary Figure 5A). Despite DNA damage, STING−/− organoids exhibited lower cleaved-PARP, indicating evasion of apoptosis.

These studies were repeated using ROS exposure over seven days and confirmed that WT organoids arrested growth or collapsed under stress, while STING−/− organoids continued proliferating (Figure 3E–F). To confirm STING's contribution to this phenomenon, pharmacologic STING blockade with C-171 rescued ROS-induced growth inhibition in WT organoids (Figure 3G). Treatment with patient-derived follicular fluid produced similar results, with WT organoids showing growth suppression while STING−/− organoids remained unaffected (Figure 3H). Furthermore, RNA-seq and GSEA analysis of WT organoids after 24-hour follicular fluid exposure revealed selective upregulation of only four significant pathways ($p<0.05$), including tumor-suppressive p53 signaling and TNFα signaling via NF-κB, both with known STING crosstalk (Figure 3I).

Together, these results indicate that STING intrinsically regulates DNA damage responses in fallopian tube epithelium through p53 activation and apoptosis induction, thereby limiting proliferation under genomic stress.

STING Overexpression in Secretory Cells Activates p53 and Apoptosis to Suppress Genomic Instability

Given that secretory cells are the established cells-of-origin for HGSC and that STING modulates both intrinsic tumor suppressive mechanisms and extrinsic immune responses, we sought to determine whether elevated STING expression in secretory murine oviductal epithelial (MOE) cells could reduce DNA damage accumulation. To address this, we generated MOE cells with STING overexpression (MOE:STING-OE) and challenged them with H2O2 to mimic follicular fluid-induced ROS. Notably, STING overexpression alone did not activate downstream signaling pathways. However, upon ROS challenge, MOE:STING-OE cells exhibited increased TBK1 phosphorylation, upregulation of cGAS-STING target genes (including IFNB1 and CXCL10), and enhanced IFNB1 promoter activity compared to scrambled controls (MOE:SCR) (Figure 4A; Supplementary Figure 6A–D). Importantly, MOE:STING-OE cells demonstrated a significant reduction in γH2AX expression following ROS exposure relative to controls (Figure 4A). Immunofluorescence analysis revealed that both MOE:SCR and MOE:STING-OE cells accumulated γH2AX foci at early time points post-ROS treatment; however, STING-overexpressing cells showed a significant resolution of γH2AX accumulation as early as 6 hours, whereas control cells continued to accumulate γH2AX through 24 hours (Figure 4B; Supplementary Figure 6E). Importantly, we found that the marked reduction in acute γH2AX accumulation was due to increased apoptosis, as STING-high cells displayed heightened sensitivity to ROS-induced stress. MOE:STING-OE cells exhibited a significantly lower H_2O_2 IC50 compared to controls and showed a diminished capacity for colony formation, indicating increased sensitivity to oxidative stress and reduced proliferative potential only in the presence of ROS challenge (Figure 4C & 4D). Furthermore, STING-high cells had significantly greater induction of apoptotic markers cleaved-caspase-3 and cleaved-PARP indicating that these cells have an increased susceptibility to cell death upon ROS challenge (Figure 4E) (Supplementary Figure 6F).

To elucidate the mechanism underlying the reduced DNA damage accumulation observed in STING-overexpressing cells, we next investigated the role of apoptosis. As ferroptosis has also been implicated in STING-induced cell death, we first assessed whether this pathway contributes to the phenotype. Analysis of ferroptosis markers—including ACSL4, NCOA4, and GPX4—following hydrogen peroxide treatment showed no increase in expression in either MOE:STING-OE or control cells, suggesting that ferroptosis is unlikely to play a significant role in this context (Supplementary Figure 6G). Nevertheless, we cannot definitively rule out ferroptosis without further experimentation. To directly test the involvement of apoptosis, we co-treated MOE:SCR and MOE:STING-OE cells with hydrogen peroxide and the pan-caspase inhibitor Z-VAD-FMK. Caspase inhibition significantly increased the hydrogen peroxide IC50 values in both cell lines and, notably, abrogated the difference between them (Supplementary Figure 6H). Consistent with these findings, western blot analysis showed that Z-VAD-FMK treatment markedly reduced levels

of the apoptotic marker cleaved-PARP (Supplementary Figure 6I). Importantly, blocking caspase activity reversed the reduction in γH2AX accumulation seen in MOE:STING-OE cells, restoring γH2AX levels to those observed in the control group. Collectively, these results indicate that apoptosis is the primary mechanism responsible for the reduction in DNA damage accumulation in STING-overexpressing MOE cells.

Having previously demonstrated that p53 activation is attenuated in STING−/− organoids—resulting in decreased apoptosis relative to the wild-type—we next assessed p53 expression and activity in MOE:STING-OE cells. Following ROS challenge, p53 expression was upregulated in MOE:STING-OE cells as early as one hour and remained elevated through six hours, with levels significantly exceeding those in scrambled controls (Figure 4F; Supplementary Figure 6J). Concordantly, key p53 target genes were robustly induced in MOE:STING-OE cells after peroxide exposure, indicating enhanced p53 pathway activation compared to controls (Figure 4G). Protein analysis also revealed increased p21 expression and a concomitant early decrease in RB phosphorylation in STING-overexpressing cells (Figure 4F; Supplementary Figure 6J). Pretreatment of MOE:SCR cells with the antioxidant N-acetylcysteine (NAC) prior to H_2O_2 exposure significantly reduced the accumulation of γH2AX, TBK1 phosphorylation, and p21, confirming that these responses are driven by oxidative stress in this system (Supplementary Figure 6K). Notably, of the pro-apoptotic p53 target genes tested, only NOXA was preferentially upregulated in MOE:STING-OE cells, which aligns with recent studies on cGAS-STING-mediated apoptotic priming (Figure 4H)[40]. Consistent with these molecular findings, Annexin V staining demonstrated that STING-overexpressing cells undergo significantly higher levels of apoptosis compared to wild-type controls (Figure 4I).

STING-High Cells Restrain DNA Damage Accumulation Through TNFα-Mediated Paracrine Signaling

Our data indicate that high STING expression can intrinsically limit DNA damage accumulation by regulating p53 activity. However, it remains unclear whether STING signaling can also reduce genomic instability in neighboring STING-low cells through extrinsic, paracrine mechanisms. Notably, our earlier results showed that primary patient ciliated cells reduced γH2AX accumulation not only in themselves, but also in neighboring secretory cells (Figure 1D).Thus, we hypothesized that STING-high cells protect neighboring cells via secreted factors. To test this, we co-cultured MOE:SCR cells with or without MOE:STING-OE cells and exposed them to hydrogen peroxide, mimicking the post-ovulatory oxidative environment (Figure 5A; Supplementary Figure 7A). MOE:SCR cells co-cultured with MOE:STING-OE cells exhibited significantly fewer γH2AX foci after 6 hours and had a marked reduction in RAD51 foci by 3 hours, suggesting a shift from DNA repair to apoptosis compared to controls (Figure 5B). Concordantly, co-cultured STING-low cells showed significantly higher apoptosis (Figure 5C), indicating that STING-high cells promote apoptosis and reduce genomic instability in neighboring cells. To test if secreted factors alone were sufficient, we treated MOE:SCR cells with conditioned media from peroxide-treated MOE:STING-OE (SO-CM) or control (SCR-CM) cells (Figure 5D). Exposure to SO-CM resulted in reduced γH2AX and increased cleaved-PARP and cleaved-caspase-8, indicative of extrinsic apoptosis (Figure 5E; Supplementary

Figure 7B). However, SO-CM did not further activate the STING or p53 pathways compared to SCR-CM, suggesting that other mechanisms mediate this pro-apoptotic effect (Figure 5E; Supplementary Figure 7C).

Recent studies have demonstrated that activation of the cGAS-STING pathway in breast cancer cells triggers secretion of TNF-α, promoting a pro-apoptotic microenvironment. Notably, this pathway was among the most significantly induced in secretory cells exposed to patient-derived follicular fluid (Figure 3I)[40]; thus, we assessed TNF-α expression in our model. Following ROS challenge, MOE:STING-OE cells showed significantly increased TNF-α mRNA levels compared to controls (Figure 5F). Conditioned media from these cells (SO-CM) enhanced phosphorylation of JNK and accumulation of cleaved-caspase-8, markers of TNF-α–mediated extrinsic apoptosis (Figure 5E). Cells exposed to SO-CM were also more sensitive to peroxide-induced cell death, as shown by colony formation and viability assays (Figures 5G & 5H). Importantly, pre-incubation of SO-CM with TNF-α neutralizing antibody (TNFi) restored cell viability and reduced markers of apoptosis, while increasing γH2AX levels to those seen with SCR-CM (Figures 5G–I; Supplementary Figure 7B). Additionally, SO-CM treatment upregulated NOXA in STING-low cells, potentially lowering their apoptotic threshold and facilitating clearance of unstable cells (Figure 5J). Together, these data indicate that STING-high cells promote paracrine, TNF-α–mediated apoptotic priming to protect neighboring STING-low cells from DNA damage following genotoxic stress.

To confirm our findings that the extrinsic, anti-proliferative effects exerted by STING-high cells are carried out independent of STING activity in their recipient cells, we incubated WT and STING−/− organoids with SO-CM and SCR-CM along with peroxide and measured viability over time. Low-dose peroxide significantly attenuated growth in WT organoids, and this reduction was more pronounced in the presence of SO-CM, but not SCR-CM (Figure 5K). As expected, high-dose peroxide induced cell death in all conditions in WT organoids (Supplementary Figure 7D). Interestingly, the STING −/− organoids showed no change in the presence of high dose peroxide treatment or SCR-CM, however in the presence of SO-CM, viability significantly decreased (Figure 5L). suggesting that STING-high cells can influence the microenvironment and promote the clearance of genomically unstable cells through paracrine signaling, even if those cells lack intrinsic STING activity.

p53 deficient cells are resistant to extrinsic STING-mediated cell death

Our data has revealed that the STING pathway activity provides protection to low-STING expressing secretory cells of the fallopian tube from excessive DNA damage accumulation by promoting programmed cell death. However, it remains unclear how early p53-deficient lesions (p53 signatures) in the FTE, which are the precursors to HGSC, respond to STING-mediated extrinsic apoptotic pressure. This is especially important to understand given that all the patient samples we analyzed showed a significant loss of STING within these lesions, however, they were often flanked by normal FTE containing ciliated cells with high STING expression (Figure 1C). Our data showed that STING-driven extrinsic pro-apoptotic signaling robustly activated the p53 cascade in recipient cells (Figure 5E, Supplementary Figure 7A–B). To test whether STING-high cells retain anti-tumor activity in the absence

of p53, we generated TP53-null murine oviductal organoids (p53−/−). Upon peroxide exposure, p53−/− organoids accumulated significantly more γH2AX but failed to activate p53 target genes, confirming loss of p53 pathway function (Figure 6A–B, Supplementary Figure 8A). Notably, these organoids also showed reduced TBK phosphorylation after peroxide challenge, indicating impaired STING signaling and supporting prior reports that p53 function is essential for full STING activity[60,61]. Next, we exposed p53−/− organoids to conditioned media from MOE:STING-OE or MOE:SCR cells together with high-dose peroxide for seven days. Neither SO-CM nor SCR-CM attenuated p53−/− organoid growth, demonstrating that recipient cell p53 functionality is required for STING-induced paracrine apoptotic priming. These findings highlight that loss of p53 disables both intrinsic and extrinsic STING-mediated tumor-suppressive mechanisms (Figure 6C).

To further explore how loss of p53 function may make cells resistant to STING-driven paracrine apoptotic priming, we employed MOE cells with an overexpression of mutant p53 (MOE:$P53^{R273H}$). We exposed these p53 mutant oviductal cells to conditioned media from MOE:SCR and MOE:STING-OE cells that had been challenged with H_2O_2 and measured viability. Whereas SO-CM was able to increase sensitivity to H_2O_2 in MOE:SCR cells (Figure 5G), we observed no difference in viability in MOE:$P53^{R273H}$ cells exposed to both conditioned medias (Figure 6D). Importantly, unlike MOE-WT cells, MOE:$P53^{R273H}$ cells showed no significant increase in cleaved PARP upon exposure to STING-high conditioned media (SO-CM), indicating a lack of pro-apoptotic response despite a clear increase in γH2AX (Figure 6E). This suggests that mutant p53 abrogates the apoptotic benefit normally conferred by STING-high paracrine signaling. Interestingly, SO-CM did still induce JNK phosphorylation and caspase 8 cleavage, indicating that the extrinsic cell death pathway is still active however this was not able to induce significant apoptosis (Figure 6E) (Supplementary Figure 8B). Next, we examined the expression of several of p53 pro-apoptotic target genes. We found that the p53 mutant cells exhibited significantly lower NOXA expression at baseline and were incapable of inducing NOXA after exposure to SO-CM in contrast to MOE:SCR cells, consistent with previous reports highlighting the importance of NOXA in mediating the STING-TNFα induced extrinsic cell death axis (Figure 6F)[40].

Discussion

Ciliated cells are critical for maintaining fertility by facilitating post-ovulatory ovum transport through the fallopian tube; however, they are not considered the cell of origin of HGSC and thus their role in tumorigenesis has been largely overlooked. Herein, we provide evidence that their tumor-suppressive role lies in preserving STING expression within the tubal microenvironment, serving as a critical mechanism for limiting DNA damage accumulation. Our findings suggest that STING-high ciliated cells serve as an early protective barrier in FTE by eliminating stressed or damaged neighboring cells through paracrine signaling. In contrast, secretory cells, which are inherently STING-low, are less equipped to engage this surveillance mechanism. Consequently, following p53 mutation and loss of function—the initiating event for HGSC—secretory cells are able to evade STING-mediated elimination, underscoring the essential protective contribution of ciliated cells prior to p53 loss.

The number of ciliated cells in the FTE fluctuate with the estrus cycle, peaking during the follicular phase and declining after ovulation as the luteal phase progresses, particularly in the distal end of the fallopian tube[62,63]. These dynamic shifts in the epithelial population are primarily driven by changes in estrogen and progesterone secretion from the ovary; however, ciliated cell populations are diminished with age[22,23,64–66]. Perimenopausal decline in estrogen production may contribute to age-related decline in ciliated cells[67,68].The timing of this physiological change in the FTE coincides with its exposure to increasingly genotoxic follicular fluid and precedes the median age of onset of HGSC[12,18,20]. Moreover, the recent observation that women with fewer tubal ciliated cells, regardless of age, are at a higher risk for developing HGSC has bolstered the hypothesis that ciliated cells may play a key role in protecting the FTE from genotoxic stress during reproductive age[22,23]. Our data support a sentinel role for ciliated cells and implicate STING as the key driver of both its intrinsic and extrinsic tumor suppressive functions.

The divergent DNA damage response of secretory and ciliated epithelial cells was first described by Levanon et al., who observed that ciliated cells accumulate far less γH2AX after ionizing radiation exposure compared to secretory cells[25]. Similarly, we demonstrate that the presence of ciliated cells in a mixed population of primary patient-derived epithelial cells is sufficient to reduce γH2AX accumulation. Importantly, ablation of the cGAS-STING signaling pathway is sufficient to abrogate the protective phenotype provided by ciliated cells. These findings indicate that the ciliated cells' capacity to reduce DNA damage accumulation is contingent upon active STING signaling. Mechanistically, STING pathway activation is known to induce strategic elimination of cells in crisis through immune-cell mediated killing, senescence, ferroptosis, necroptosis, and apoptosis[44,69–71]. Furthermore, cell fate is predicated on cellular context and signaling strength[43–45,72,73]. Here we demonstrate that the fallopian tube epithelium preferentially responds to acute genotoxic stress via STING-driven apoptosis as a strategy to reduce the accumulation of genomic instability.

There is growing evidence for bidirectional crosstalk and, perhaps, co-dependency between the STING and p53 pathways. Recent studies have demonstrated that the canonical tumor suppressive function of p53 is inextricably tied to the signaling competence of the STING pathway[60,61,74]. In both cancerous and non-cancerous contexts, knock-out of STING or its various pathway constituents impaired p53 activity and thus restrained canonical DNA damage responses to genotoxic stressors, resulting in unabated cell growth accompanied by unresolved genomic instability[60,61]. Congruently, our investigation revealed that knockout of STING diminished oviductal apoptotic response to ovulatory stress *in vivo*. Additionally, *in vitro* study of oviductal organoids from these models revealed loss of STING resulted in unmitigated cell growth, increased DNA damage, and reduced p53 activity in response to genomic stress. Similarly, we show that overexpression of STING in murine secretory cells enhanced p53 signaling and coincided with increased apoptosis when exposed to ROS. While these data strongly suggest STING pathway activity underlies p53 function, recent studies have indicated that the p53 pathway may reciprocally impact STING pathway efficacy. p53 indirectly influences STING pathway activation through the regulation of cytoplasmic endonuclease TREX1 which can deplete the pool of available substrate for cGAS, blunting the pathway[74]. Additionally, DNA damaging agents synergize with STING

pathway mediator IRF3 to hyperactivate p53 and induce cell death, while loss of p53 is sufficient to rescue cell death in this model[61]. These data collectively suggest that p53 and STING engage in an inextricable co-functionality to affect an intrinsic tumor suppressive response to genomic instability.

Here we describe for the first time that STING's extrinsic pro-apoptotic function also relies on p53 signaling integrity in recipient cells. STING-high cells fail to induce anti-tumor effects in p53-deficient cells, which accumulate DNA damage without activating apoptosis. This resistance may contribute to the progression of HGSC once p53 function is lost, thus converting a non-progressive STIC lesion to a progressive lesion. Our data corroborates recent findings that NOXA acts as the key mediator of STING's extrinsic pro-apoptotic mechanism[40]. NOXA is a well-known p53 target gene; unsurprisingly, mutation or loss of p53 in oviductal cells is accompanied by a concomitant drop in NOXA expression suggesting that coincidental loss of NOXA may contribute to the ability of p53 deficient lesions (such as p53 signatures or STICs) to circumvent STING's pro-apoptotic influence on the microenvironment. Our data shows the importance of competent STING signaling the microenvironment and that loss of p53 can induce tolerance of extrinsic STING-driven tumor suppression. Additional research is needed to explore the importance of p53 functionality to indirectly influence STING's pro-apoptotic extrinsic function. Study of the extrinsic anti-tumor function of the STING pathway has mostly revolved around its ability to induce an anti-cancer immune response[73,75]. However, our data indicate that STING activity in the fallopian tube acts as an extrinsic tumor suppressor, independent of the immune system.

Recent work by Lohard et al. demonstrated that STING activation triggers paracrine apoptotic priming via TNF-α and NOXA[40]. Here, we show this mechanism operates in the FTE, where STING-high cells secrete TNF-α to promote apoptotic clearance of genomically unstable neighbors and reduce DNA damage. This response is clinically relevant, as TNF signaling is upregulated in FTE exposed to follicular fluid and contributes to genomic instability. Conditioned media or co-culture with STING-high cells induces apoptosis and reduces γH2AX in STING-low cells exposed to ROS, with NOXA upregulation confirming its key role. Critically, this tumor-suppressive axis depends on functional p53, and is compromised in p53-deficient lesions. Future studies should clarify how STING, TNF-α, NOXA, and p53 collaborate to maintain epithelial homeostasis, and assess the therapeutic potential of targeting this pathway, particularly in settings where p53 function is lost. Combining STING agonists with DNA-damaging agents, BH3 mimetics, p53 reactivators, or immune checkpoint blockade may help restore anti-tumor responses.

In conclusion, our findings reveal that STING serves as a critical tumor-suppressive gatekeeper in the FTE by safeguarding against the accumulation of DNA damage through both intrinsic and extrinsic mechanisms. We uncovered a lineage-specific pattern of STING expression where in ciliated epithelial cells exhibit higher STING levels compared to secretory cells. The reduction in STING expression in p53 signatures, STICs and HGSCs reflects a shift in epithelial composition, marked by the loss of STING-high ciliated cells and expansion of secretory-derived tumor cells. Early depletion of STING expression may thus compromise epithelial integrity, promote genomic instability, and promote

the progression of STIC lesions to HGSC. Understanding the mechanisms underlying STING exclusion and its functional consequences could inform novel strategies for HGSC prevention and therapeutic intervention.

Supplementary Material

Refer to Web version on PubMed Central for supplementary material.

ACKNOWLEDGEMENTS

Research reported in this publication was supported by the National Cancer Institute of the National Institutes of Health under Award Number R01CA197780 (AD), CA240301 (JEB), CA240423 (JEB), DE026728 (LL), R01CA226756 (KRC), 2T32CA009676–31 (JAC), Tina's Wish Rising Star Fellowship (MSR), the Department of Veterans Administration Merit Awards VA-ORD BX004974 and VA-ORD BX006020 (SO), the Office of the Assistant Secretary of Defense for Health Affairs through the Ovarian Cancer Research Program Awards W81XWH-22–1-0631 and HT9425–24-1–0193 (SO), W81XWH-22–1-0852 (RD), and National Center for Advancing Translational Sciences UCLA CTSI Grant UL1TR001881 (MSR and SO). Further acknowledgments are extended to the generous donors and Foundations who have financially supported our ovarian cancer research in the DiFeo Lab, striving to improve the outcomes of HGSC patients, including The Silver Family Foundation, The Barbara Robson Foundation, and The Debra A. and Dean A. Frick Ovarian Cancer Research Fund. As well as the Gray Foundation grants which supported the Drapkin lab and Sandy Rollman Ovarian Cancer Foundation which supported the Orsulic lab. The content is solely the responsibility of the authors and does not necessarily represent the official views of the National Institutes of Health (NIH). We are grateful for the contributions provided by the following cores at the University of Michigan and Rogel Cancer Center (P30CA046592): Center for Chemical Genomics at the Life Sciences Institute, Frankel Cardiovascular Center Cardiovascular Regeneration Core Laboratory, Flow Cytometry Core, Pharmacokinetics Core, Cancer Data Science, and Viral Vector Core. Thanks to Martin Clasby, Ph.D. for input on chemical descriptions. Illustrations were created with Biorender. Thanks to Dr. Erica Marsh, whose repository provided the FF samples and Rong Wu who helped to execute the experiments that include follicular fluid.

Bibliography

1. Siegel RL, Giaquinto AN & Jemal A Cancer statistics, 2024. CA: A Cancer Journal for Clinicians 74, 12–49 (2024). [PubMed: 38230766]
2. Bowtell DD et al. Rethinking ovarian cancer II: reducing mortality from high-grade serous ovarian cancer. Nat Rev Cancer 15, 668–679 (2015). [PubMed: 26493647]
3. Labidi-Galy SI et al. High grade serous ovarian carcinomas originate in the fallopian tube. Nature Communications 8, 1–11 (2017).
4. Kindelberger DW et al. Intraepithelial Carcinoma of the Fimbria and Pelvic Serous Carcinoma: Evidence for a Causal Relationship. The American Journal of Surgical Pathology 31, 161–169 (2007). [PubMed: 17255760]
5. Lee Y et al. A candidate precursor to serous carcinoma that originates in the distal fallopian tube. J. Pathol. 211, 26–35 (2007). [PubMed: 17117391]
6. Kuhn E et al. TP53 mutations in serous tubal intraepithelial carcinoma and concurrent pelvic high-grade serous carcinoma—evidence supporting the clonal relationship of the two lesions. J Pathol 226, 421–426 (2012). [PubMed: 21990067]
7. Eckert MA et al. Genomics of ovarian cancer progression reveals diverse metastatic trajectories including intraepithelial metastasis to the fallopian tube. Cancer Discov 6, 1342–1351 (2016). [PubMed: 27856443]
8. Emori MM & Drapkin R The hormonal composition of follicular fluid and its implications for ovarian cancer pathogenesis. Reprod Biol Endocrinol 12, 60 (2014). [PubMed: 24997727]
9. Bahar-Shany K et al. Exposure of fallopian tube epithelium to follicular fluid mimics carcinogenic changes in precursor lesions of serous papillary carcinoma. Gynecologic Oncology 132, 322–327 (2014). [PubMed: 24355484]

10. King SM et al. The impact of ovulation on fallopian tube epithelial cells: evaluating three hypotheses connecting ovulation and serous ovarian cancer. Endocrine-Related Cancer 18, 627–642 (2011). [PubMed: 21813729]
11. Fathalla MF INCESSANT OVULATION—A FACTOR IN OVARIAN NEOPLASIA ? The Lancet 298, 163 (1971).
12. Salvi A et al. Follicular fluid aids cell adhesion, spreading in an age independent manner and shows an age-dependent effect on DNA damage in fallopian tube epithelial cells. Heliyon 10, e27336 (2024). [PubMed: 38501015]
13. Zhu M et al. Effects of Follicular Fluid on Physiological Characteristics and Differentiation of Fallopian Tube Epithelial Cells Implicating for Ovarian Cancer Pathogenesis. Int J Mol Sci 24, 10154 (2023). [PubMed: 37373301]
14. Huang H-S et al. Mutagenic, surviving and tumorigenic effects of follicular fluid in the context of p53 loss: initiation of fimbria carcinogenesis. Carcinogenesis 36, 1419–1428 (2015). [PubMed: 26363031]
15. Walters KA et al. Steroid profiles by liquid chromatography-mass spectrometry of matched serum and single dominant ovarian follicular fluid from women undergoing IVF. Reproductive BioMedicine Online 38, 30–37 (2019). [PubMed: 30527851]
16. Palma-Vera SE, Schoen J & Chen S Periovulatory follicular fluid levels of estradiol trigger inflammatory and DNA damage responses in oviduct epithelial cells. PLOS ONE 12, e0172192 (2017). [PubMed: 28231273]
17. Ishak CA et al. Chronic Viral Mimicry Induction following p53 Loss Promotes Immune Evasion. Cancer Discovery 15, 793–817 (2025). [PubMed: 39776167]
18. Siegel RL, Miller KD, Wagle NS & Jemal A Cancer statistics, 2023. CA: A Cancer Journal for Clinicians 73, 17–48 (2023). [PubMed: 36633525]
19. Dilley J et al. Ovarian cancer symptoms in pre-clinical invasive epithelial ovarian cancer – An exploratory analysis nested within the UK Collaborative Trial of Ovarian Cancer Screening (UKCTOCS). Gynecologic Oncology 179, 123–130 (2023). [PubMed: 37980767]
20. Dao F et al. Characteristics of 10-year survivors of high-grade serous ovarian carcinoma. Gynecol Oncol 141, 260–263 (2016). [PubMed: 26968641]
21. Debbarh H et al. Antioxidant activities and lipid peroxidation status in human follicular fluid: age-dependent change. Zygote 29, 490–494 (2021). [PubMed: 33910658]
22. Li J et al. Secretory cell expansion with aging: Risk for pelvic serous carcinogenesis. Gynecologic Oncology 131, 555–560 (2013). [PubMed: 24060413]
23. Tao T et al. Loss of tubal ciliated cells as a risk for “ovarian” or pelvic serous carcinoma. Am J Cancer Res 10, 3815–3827 (2020). [PubMed: 33294269]
24. Richardson MT, Recouvreux MS, Karlan BY, Walts AE & Orsulic S Ciliated Cells in Ovarian Cancer Decrease with Increasing Tumor Grade and Disease Progression. Cells 11, 4009 (2022). [PubMed: 36552773]
25. Levanon K et al. Primary ex vivo cultures of human fallopian tube epithelium as a model for serous ovarian carcinogenesis. Oncogene 29, 1103–1113 (2010). [PubMed: 19935705]
26. Coan M et al. Exploring the Role of Fallopian Ciliated Cells in the Pathogenesis of High-Grade Serous Ovarian Cancer. International Journal of Molecular Sciences 19, 2512 (2018). [PubMed: 30149579]
27. Kobayashi T et al. CEP164 Deficiency Causes Hyperproliferation of Pancreatic Cancer Cells. Front Cell Dev Biol 8, 587691 (2020). [PubMed: 33251215]
28. Han Y-G et al. Dual and opposing roles of primary cilia in medulloblastoma development. Nat Med 15, 1062–1065 (2009). [PubMed: 19701203]
29. Seeley ES, Carrière C, Goetze T, Longnecker DS & Korc M Pancreatic Cancer and Precursor Pancreatic Intraepithelial Neoplasia Lesions Are Devoid of Primary Cilia. Cancer Research 69, 422–430 (2009). [PubMed: 19147554]
30. Huvila J et al. STING pathway expression in low-grade serous carcinoma of the ovary: an unexpected therapeutic opportunity? J Pathol Clin Res 7, 548–555 (2021). [PubMed: 34138519]

31. Menz A et al. Stimulator of Interferon Genes Protein (STING) Expression in Cancer Cells: A Tissue Microarray Study Evaluating More than 18,000 Tumors from 139 Different Tumor Entities. Cancers 16, 2425 (2024). [PubMed: 39001487]
32. Chen C & Xu P Cellular functions of cGAS-STING signaling. Trends in Cell Biology 33, 630–648 (2023). [PubMed: 36437149]
33. Hopfner K-P & Hornung V Molecular mechanisms and cellular functions of cGAS–STING signalling. Nat Rev Mol Cell Biol 21, 501–521 (2020). [PubMed: 32424334]
34. Kwon J & Bakhoum SF The Cytosolic DNA-Sensing cGAS–STING Pathway in Cancer. Cancer Discovery 10, 26–39 (2020). [PubMed: 31852718]
35. Jiang M et al. cGAS-STING, an important pathway in cancer immunotherapy. J Hematol Oncol 13, 81 (2020). [PubMed: 32571374]
36. Zheng J et al. Comprehensive elaboration of the cGAS-STING signaling axis in cancer development and immunotherapy. Mol Cancer 19, 133 (2020). [PubMed: 32854711]
37. Kumar V, Bauer C & Stewart JH Cancer cell-specific cGAS/STING Signaling pathway in the era of advancing cancer cell biology. European Journal of Cell Biology 102, 151338 (2023). [PubMed: 37423035]
38. Murthy AMV, Robinson N & Kumar S Crosstalk between cGAS–STING signaling and cell death. Cell Death Differ 27, 2989–3003 (2020). [PubMed: 32948836]
39. Yang J et al. STING in tumors: a focus on non-innate immune pathways. Front Cell Dev Biol 11, 1278461 (2023). [PubMed: 37965570]
40. Lohard S et al. STING-dependent paracriny shapes apoptotic priming of breast tumors in response to anti-mitotic treatment. Nat Commun 11, 259 (2020). [PubMed: 31937780]
41. Zhang C et al. Structural basis of STING binding with and phosphorylation by TBK1. Nature 567, 394–398 (2019). [PubMed: 30842653]
42. Paludan SR, Reinert LS & Hornung V DNA-stimulated cell death: implications for host defence, inflammatory diseases and cancer. Nat Rev Immunol 19, 141–153 (2019). [PubMed: 30644449]
43. Gulen MF et al. Signalling strength determines proapoptotic functions of STING. Nat Commun 8, 427 (2017). [PubMed: 28874664]
44. Li T & Chen ZJ The cGAS–cGAMP–STING pathway connects DNA damage to inflammation, senescence, and cancer. Journal of Experimental Medicine 215, 1287–1299 (2018). [PubMed: 29622565]
45. Kabelitz D et al. Signal strength of STING activation determines cytokine plasticity and cell death in human monocytes. Sci Rep 12, 17827 (2022). [PubMed: 36280676]
46. Guo Q et al. STING promotes senescence, apoptosis, and extracellular matrix degradation in osteoarthritis via the NF-κB signaling pathway. Cell Death Dis 12, 1–14 (2021). [PubMed: 33414393]
47. Knarr M et al. miR-181a initiates and perpetuates oncogenic transformation through the regulation of innate immune signaling. Nature Communications 11, 3231 (2020).
48. Ulrich ND et al. Cellular heterogeneity of human fallopian tubes in normal and hydrosalpinx disease states identified by scRNA-seq. Dev Cell 57, 914–929.e7 (2022). [PubMed: 35320732]
49. Weigert M et al. A cell atlas of the human fallopian tube throughout the menstrual cycle and menopause. Nat Commun 16, 372 (2025). [PubMed: 39753552]
50. Izar B et al. A single-cell landscape of high-grade serous ovarian cancer. Nat Med 26, 1271–1279 (2020). [PubMed: 32572264]
51. Hu Y et al. INHBA(+) cancer-associated fibroblasts generate an immunosuppressive tumor microenvironment in ovarian cancer. NPJ Precis Oncol 8, 35 (2024). [PubMed: 38360876]
52. Lõhmussaar K et al. Assessing the origin of high-grade serous ovarian cancer using CRISPR-modification of mouse organoids. Nature Communications 11, 2660 (2020).
53. Wu R et al. Impact of oviductal versus ovarian epithelial cell of origin on ovarian endometrioid carcinoma phenotype in the mouse: Oviductal versus ovarian epithelial transformation in mice. J. Pathol. 240, 341–351 (2016). [PubMed: 27538791]
54. Zhai Y et al. High-grade serous carcinomas arise in the mouse oviduct via defects linked to the human disease. J Pathol 243, 16–25 (2017). [PubMed: 28608929]

55. Dipali SS, Suebthawinkul C, Burdette JE, Pavone ME & Duncan FE Human follicular fluid elicits select dose- and age-dependent effects on mouse oocytes and cumulus–oocyte complexes in a heterologous in vitro maturation assay. Mol Hum Reprod 29, gaad039 (2023). [PubMed: 37950499]
56. Subramanian A et al. Gene set enrichment analysis: A knowledge-based approach for interpreting genome-wide expression profiles. Proc Natl Acad Sci U S A 102, 15545–15550 (2005). [PubMed: 16199517]
57. Colina JA et al. Reduced PAX2 expression in murine fallopian tube cells enhances estrogen receptor signaling. Carcinogenesis 41, 646–655 (2020). [PubMed: 31271204]
58. Avelar RA et al. Small-Molecule–Mediated Stabilization of PP2A Modulates the Homologous Recombination Pathway and Potentiates DNA Damage-Induced Cell Death. Mol Cancer Ther 22, 599–615 (2023). [PubMed: 36788429]
59. Hu Z et al. The Repertoire of Serous Ovarian Cancer Non-genetic Heterogeneity Revealed by Single-Cell Sequencing of Normal Fallopian Tube Epithelial Cells. Cancer Cell 37, 226–242.e7 (2020). [PubMed: 32049047]
60. Ranoa DRE et al. STING promotes homeostasis via regulation of cell proliferation and chromosomal stability. Cancer Res 79, 1465–1479 (2019). [PubMed: 30482772]
61. Basit A et al. The cGAS/STING/TBK1/IRF3 innate immunity pathway maintains chromosomal stability through regulation of p21 levels. Exp Mol Med 52, 643–657 (2020). [PubMed: 32284536]
62. Odor DL, Gaddum-Rosse P, Rumery RE & Blandau RJ Cyclic variations in the oviductal ciliated cells during the menstrual cycle and after estrogen treatment in the pig-tailed monkey, Macaca nemestrina. The Anatomical Record 198, 35–57 (1980). [PubMed: 7457930]
63. Donnez J, Casanas-Roux F, Caprasse J, Ferin J & Thomas K Cyclic changes in ciliation, cell height, and mitotic activity in human tubal epithelium during reproductive life. Fertility and Sterility 43, 554–559 (1985). [PubMed: 3987924]
64. Chang Y-H, Ding D-C & Chu T-Y Estradiol and Progesterone Induced Differentiation and Increased Stemness Gene Expression of Human Fallopian Tube Epithelial Cells. Journal of Cancer 10, 3028–3036 (2019). [PubMed: 31281480]
65. Okada A et al. Role of foxj1 and estrogen receptor alpha in ciliated epithelial cell differentiation of the neonatal oviduct. Journal of Molecular Endocrinology 32, 615–625 (2004). [PubMed: 15171704]
66. Ohm LA et al. Estrogen stimulates expression of FOXJ1 in the rhesus macaque fallopian tube. Fertility and Sterility 92, S116 (2009).
67. van den Beld AW et al. The physiology of endocrine systems with ageing. Lancet Diabetes Endocrinol 6, 647–658 (2018). [PubMed: 30017799]
68. Davis SR et al. Menopause. Nat Rev Dis Primers 1, 1–19 (2015).
69. Liu S & Guan W STING Signaling Promotes Apoptosis, Necrosis, and Cell Death: An Overview and Update. Mediators Inflamm 2018, 1202797 (2018). [PubMed: 30595664]
70. Berger G et al. STING activation promotes robust immune response and NK cell–mediated tumor regression in glioblastoma models. Proceedings of the National Academy of Sciences 119, e2111003119 (2022).
71. Xu Y, Chen C, Liao Z & Xu P cGAS-STING signaling in cell death: Mechanisms of action and implications in pathologies. European Journal of Immunology 53, 2350386 (2023).
72. Woo S-R et al. STING-Dependent Cytosolic DNA Sensing Mediates Innate Immune Recognition of Immunogenic Tumors. Immunity 41, 830–842 (2014). [PubMed: 25517615]
73. Zhu Y et al. STING: a master regulator in the cancer-immunity cycle. Molecular Cancer 18, 152 (2019). [PubMed: 31679519]
74. Ghosh M, Saha S, Li J, Montrose DC & Martinez LA p53 engages the cGAS/STING cytosolic DNA sensing pathway for tumor suppression. Molecular Cell 83, 266–280.e6 (2023). [PubMed: 36638783]
75. Shakfa N, Li D, Nersesian S, Wilson-Sanchez J & Koti M The STING pathway: Therapeutic vulnerabilities in ovarian cancer. Br J Cancer 127, 603–611 (2022). [PubMed: 35383278]

Statement of Significance:

STING-high ciliated fallopian tube cells function as immune-independent active guardians of genomic integrity whose loss creates a permissive niche for high-grade serous carcinoma initiation, which could inform prevention and treatment strategies.

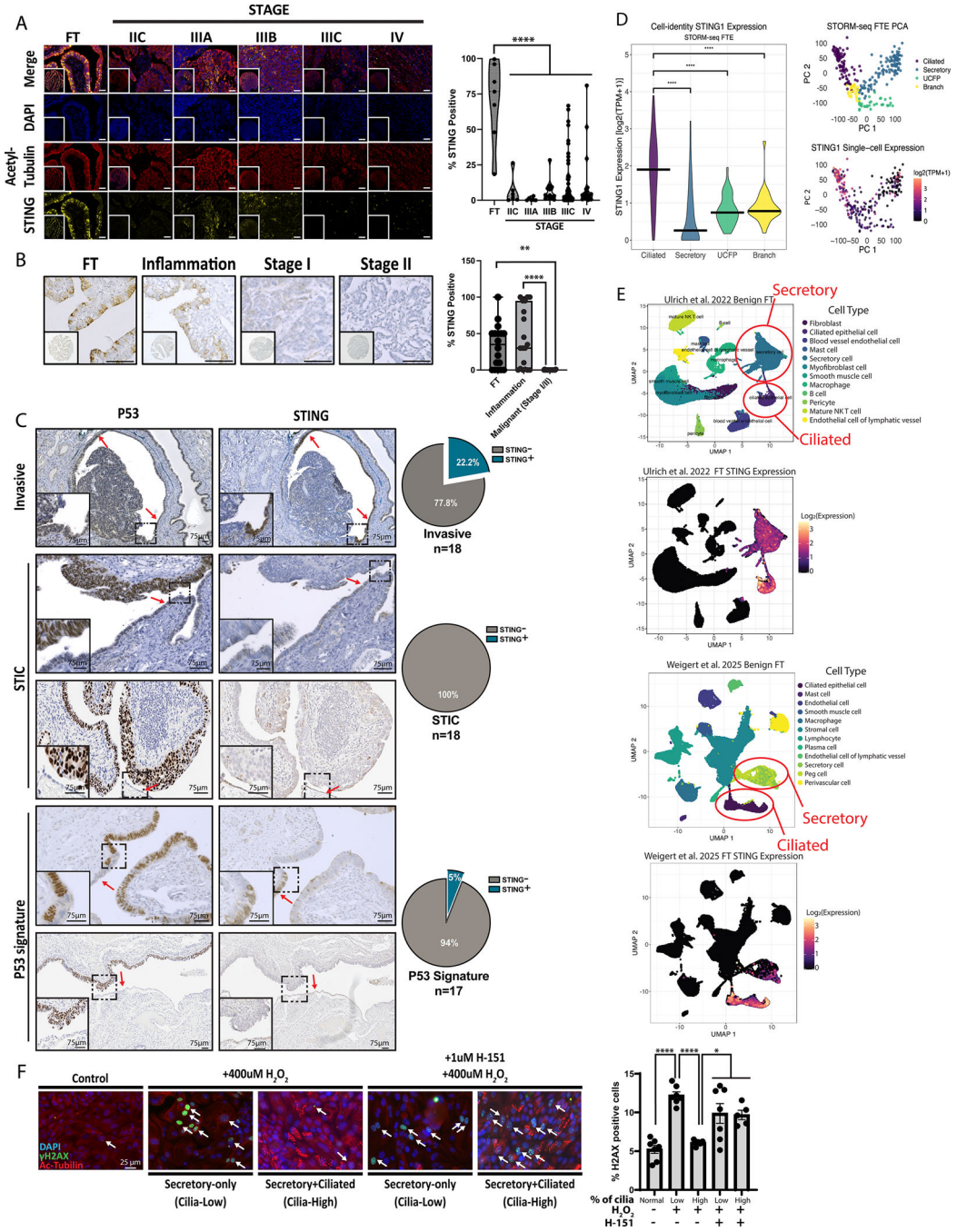

Figure 1. Ciliated Cells in the Fallopian Tube Epithelium Express STING and Its Loss Is an Early Indicator of High-Grade Serous Carcinoma.

(A) (Left) Representative immunofluorescent images of patient samples stained with DAPI (blue), Acetylated tubulin (red), and STING (yellow). (Right) corresponding quantification of percent STING positive cells across different stages of disease in including FT(n=6), IIC(n=6), III(n=3), IIIA(n=3), IIIB(n=13), IIIC(n=81), and IV(n=19). Scale bar represents 40μm. analyzed by two-sided t-test **** $p < 0.000$.

(B) Representative immunohistochemistry images of patient samples obtained from stage I and stage II tumors as well as healthy fallopian tubes and fallopian tubes from patients

with inflammatory disease stained for STING with quantification of percent STING positive cells across different stage of disease (right). Scale bar represents 75μm n≥18, analyzed by one-way ANOVA followed by a Tukey's post-hoc. * $p < 0.05$, **** $p < 0.0001$.
(C) (Left) Representative immunohistochemistry images of invasive and precancerous fallopian tube lesions (STIC and P53 signatures) from patients stained with p53 or STING. (Right) Summary of percent of samples with STING positive (STING+) and STING negative (STING-) lesions. Red arrows indicated normal adjacent FTE. </p/> (D) Single cell RNA-seq (ScRNA-seq) of patient derived fallopian tubes demonstrating that *STING* is mainly expressed in ciliated cells and correlates with ciliated cell differentiation (right).
(E) Ulrich et al. assayed four donors by 10x Genomics 3' scRNA-seq and when comparing secretory and ciliated epithelial cell types, STING1 expression is highest in ciliated cells[48].
C) Weigert et al. profiled primary human fallopian tubes from 10 donors by 10x Genomics 3' scRNA-seq, and when similarly restricted to secretory and ciliated epithelial cells in the fimbriated end of the fallopian tube, STING1 expression is highest in the ciliated cells[49].
Cluster labels provided by the original publication were used to identify shown cell types for both the Ulrich and Weigert et al. studies.
(F) Representative immunofluorescent images of primary patient FTE cells treated with 400uM peroxide, 1μM H-151, or vehicle stained with DAPI (Blue), γH2AX (Green), and Acetylated Tubulin (Red) with corresponding quantification of γH2AX. White arrows indicate γH2AX positive cells n≥5, analyzed by one-way ANOVA followed by a Tukey's post-hoc, * $p < 0.05$, **** $p < 0.0001$.

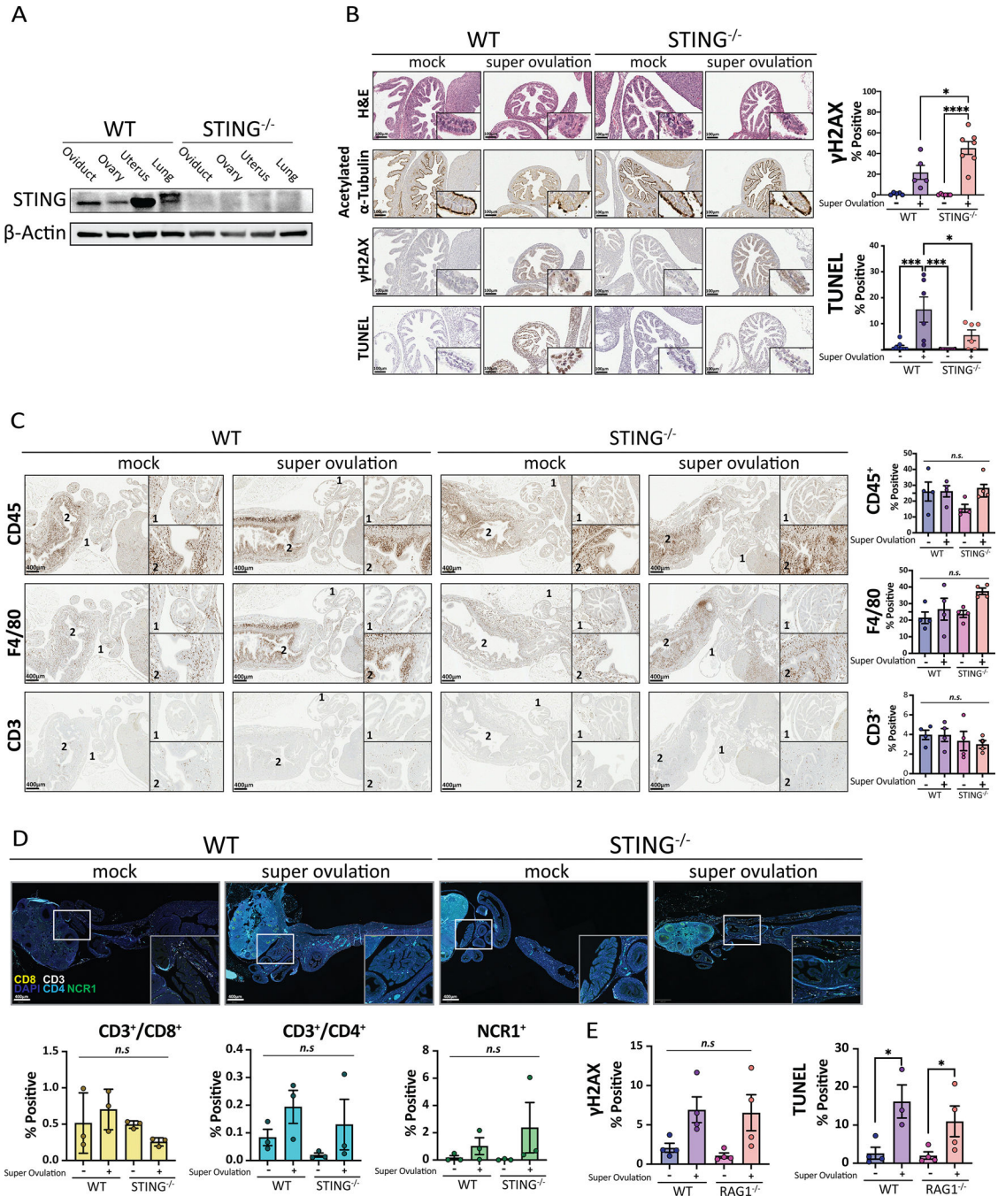

Figure 2. Loss of STING in the oviducts results in the accumulation of DNA damage in an immune-independent manner.

(A) Immunoblotting analyses of STING expression in various organs in WT and STING−/− mice (n=3).

(B) Representative images of Acetylated alpha tubulin, γH2AX, and TUNEL IHC staining of WT and STING−/− mice with and without super-ovulation along with quantification of percent positive cells. n≥5, analyzed by one-way ANOVA followed by a Tukey's post-hoc. * $p < 0.05$, **** $p < 0.0001$.

(C) Representative images of CD45, F40/80, and CD3 IHC staining of WT and STING−/− mice with and without super-ovulation along with quantification of percent positive cells. Higher magnification in panels represent the oviduct (1) and the endometrium (2). n≥4, analyzed by one-way ANOVA followed by a Tukey's post-hoc. n.s. indicates no significant difference

(D) Reproductive tracts of super-ovulated WT and STING−/− mice were analyzed by multiplex-immunofluorescence staining for CD8, CD4, CD3, DAPI, and NCR1. Expression and co-expression of markers were quantified as percentages of total cells. n≥4, analyzed by one-way ANOVA followed by a Tukey's post-hoc. n.s. indicates no significant difference

(E) WT and Rag1−/− mice were super-ovulated followed by IHC analysis for γH2AX and TUNEL in the gynecological tract. Quantification represented as percent of total cells positive for stain. n≥4, analyzed by one-way ANOVA followed by a Tukey's post-hoc. * $p < 0.05$.

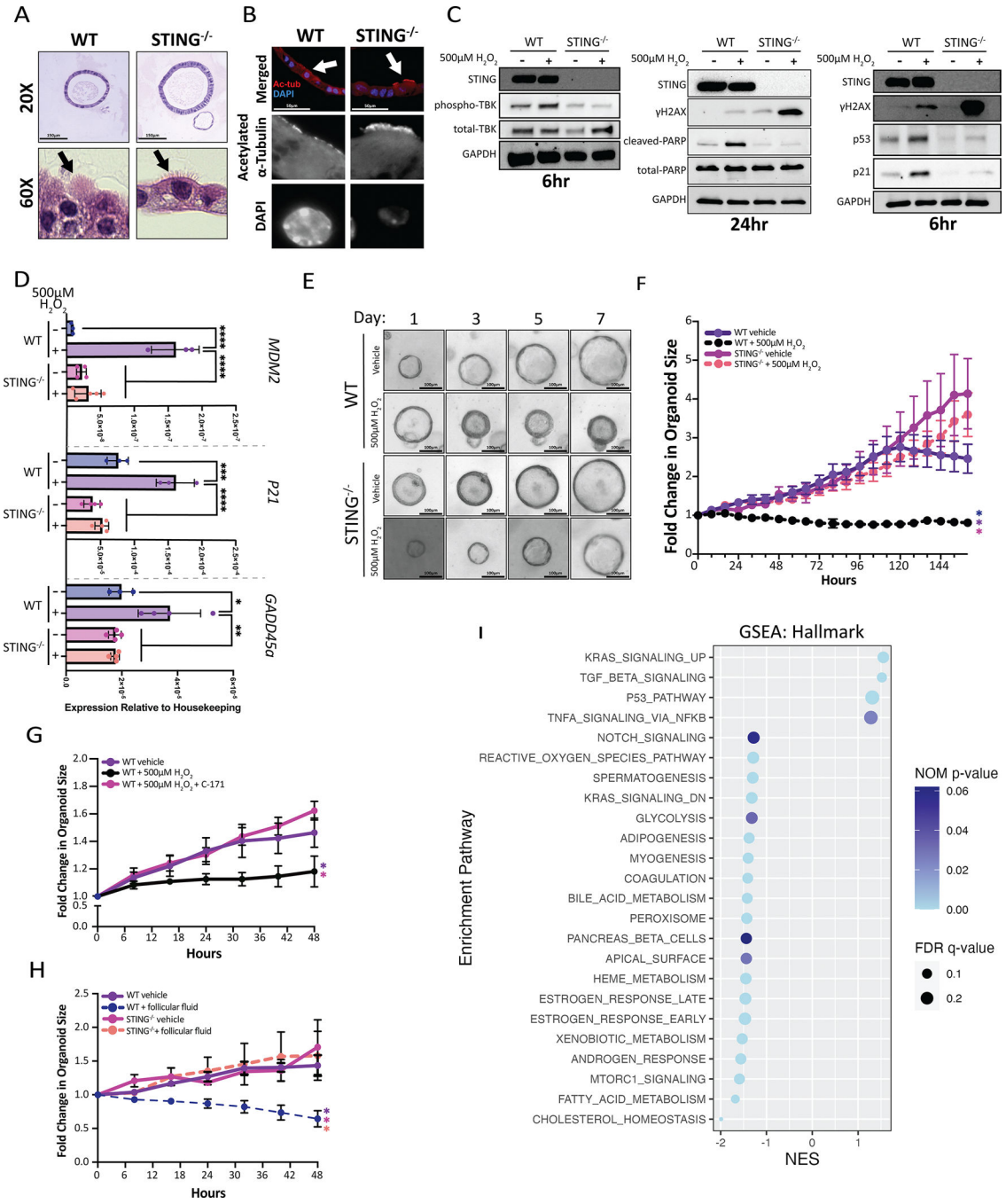

Figure 3. STING contributes to p53's DNA damage response in the FTE.

(A) Bright field images of WT and STING−/− FTE organoids. Black arrows denote presence of ciliated cells.

(B) Immunofluorescence stain of acetylated tubulin (red) and DAPI (blue) in WT and STING−/− FTE organoids. Arrows denotes ciliated cells.

(C) Immunoblot analysis for STING and its downstream targets, apoptotic markers, and p53 and its downstream targets of WT and STING−/− FTE organoids challenged with 500uM H_2O_2 at 6 and 24 hours. n≥4.

(D) qPCR analysis of p53 target gene expression in WT and STING −/− FTE organoids with and without 500uM H_2O_2. n≥5, analyzed by one-way ANOVA followed by a Tukey's post-hoc. * $p < 0.05$, ** $p < 0.01$, *** $p < 0.001$**** $p < 0.0001$.

(E) Representative images of WT and STING −/− FTE organoids incubated with H_2O_2 for 7 days and monitored by live cell imaging.

(F) Proliferation quantified by measuring organoid area over time of WT and STING −/−organoids incubated with H_2O_2. n≥5, analyzed by one-way ANOVA followed by a Tukey's post-hoc. * $p < 0.05$,

(G) Proliferation of WT FTE organoids challenged with either 500uM H_2O_2 alone or in the presence of 1uM STING inhibitor C-171 for 48 hours and monitored by live cell imaging. n≥5, analyzed by one-way ANOVA followed by a Tukey's post-hoc. * $p < 0.05$,

(H) Proliferation of WT and STING −/− FTE organoids exposed to either PBS or patient-derived follicular fluid for 48 hours and monitored by live cell imaging. n=3, analyzed by one-way ANOVA followed by a Tukey's post-hoc. * $p < 0.05$, * $p < 0.001$

(I) GSEA analysis of RNA sequencing from WT FTE organoids incubated with PBS or patient-derived follicular fluid for 24 hours.

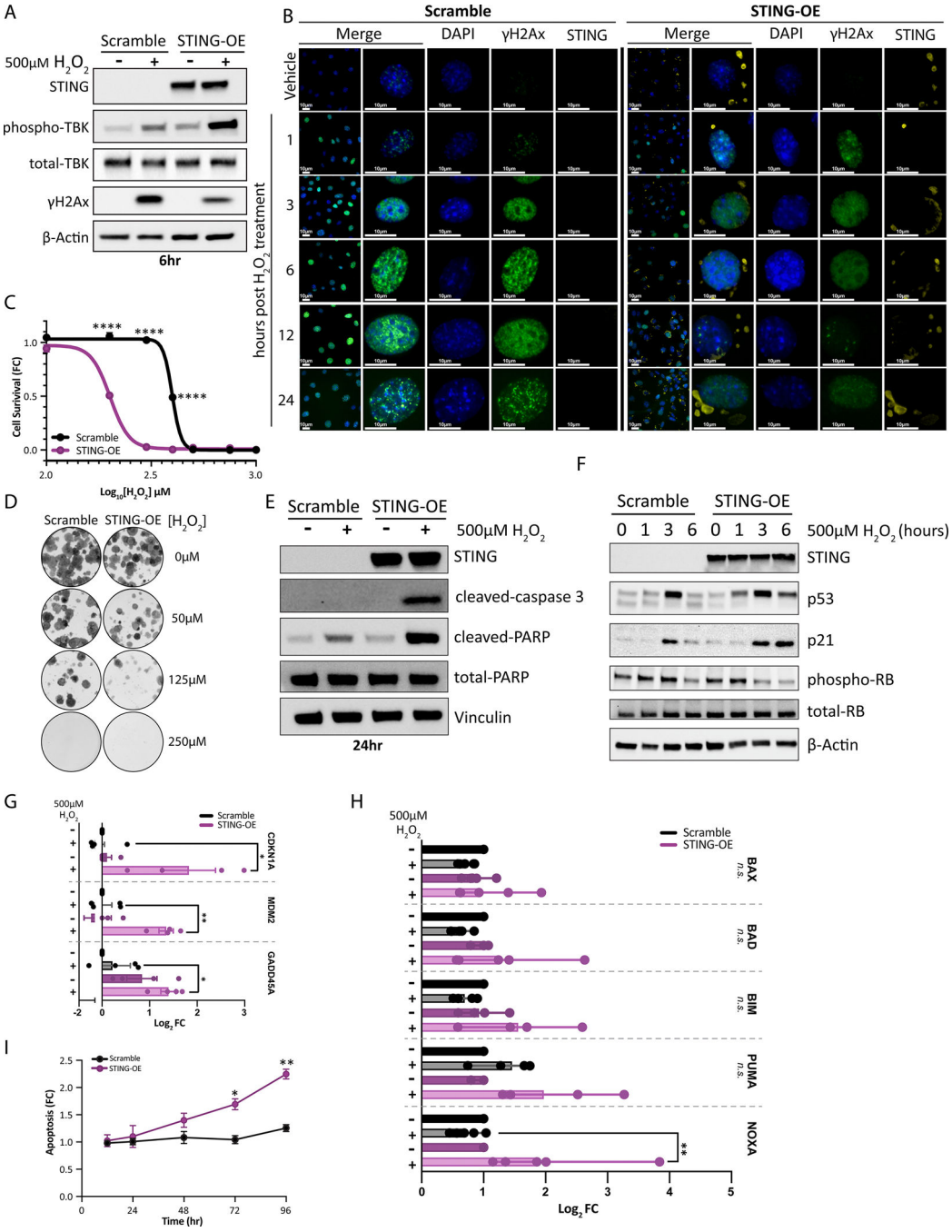

Figure 4. STING overexpression in secretory cells amplifies p53 signaling and initiates programmed cell death to prevent GI accumulation

(A) Murine oviductal epithelial cells with overexpression of either STING (MOE:STING-OE) or scramble control (MOE:SCR) were challenged with 500μM H_2O_2 for 6 hours. STING pathway activity and DNA damage accumulation were analyzed by immunoblot. n=5

(B) MOE:SCR and MOE:STING-OE cells were challenged with 500μM H_2O_2 then fixed and stained with DAPI (blue), γH2AX (green), and STING (yellow) and imaged by lightsheet microscopy n≥8

(C) Cellular viability of MOE:SCR and MOE:STING-OE cells treated with 500μM H_2O_2 for 5 days. n=4, analyzed by two-sided t-test. **** $p < 0.0001$
(D) Representative images of colony forming efficiency of MOE:SCR and MOE:STING-OE cells treated with 500μM H_2O_2 for 7 days. n=3
(E,F) Immunoblots for apoptotic markers (F) and p53 and its downstream targets (E) in MOE:SCR and MOE:STING-OE cells challenged with 500μM H_2O_2 n≥3
(G) mRNA expression of p53 target genes assessed by qPCR. n=4, analyzed by two-sided t-test * $p < 0.05$, ** $p < 0.01$
(H) mRNA expression of key apoptotic mediators regulated by p53 in cells were exposed to 500μM H_2O_2. n=4, analyzed by two-sided t-test * $p < 0.05$, ** $p < 0.01$
(I) Live cell apoptosis of MOE:SCR and MOE:STING-OE cells was monitored for 96 hours after 500μM H_2O_2 treatment using ApoLive-Glo multiplex assay. n=3, analyzed by two-sided t-test. * $p < 0.05$, ** $p < 0.01$

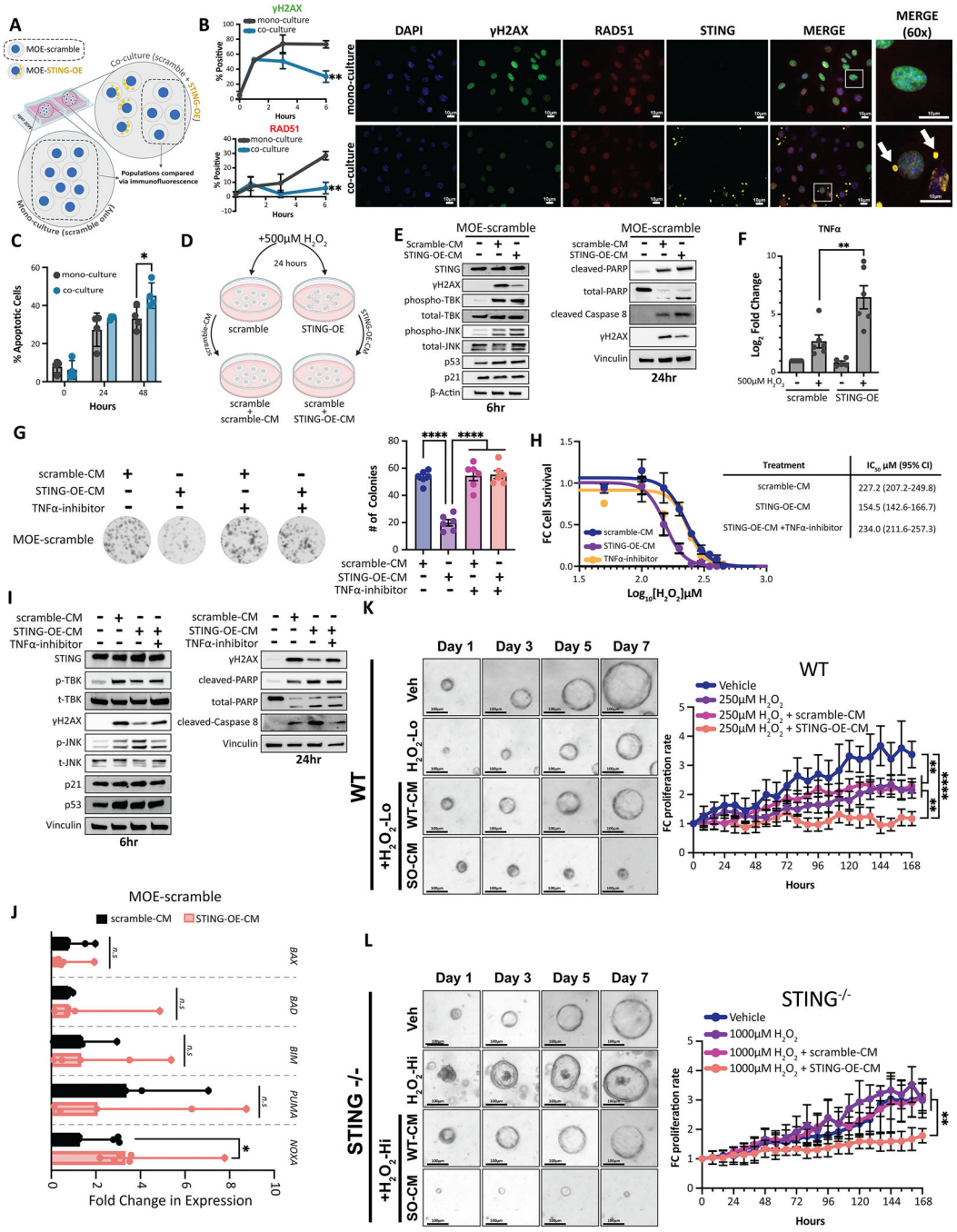

Figure 5. High STING-expressing cells protect STING-low cells from DNA damage accumulation via TNFα-mediated extrinsic paracrine signaling

(A) Experimental design for MOE:SCR and MOE:STING-OE co-culture. MOE:SCR cells with or without MOE:STING-OE cells were plated into chamber slides and challenged with 500μM H2O2. Chamber slides were fixed after 1, 3, and 6 hours of exposure and analyzed by immunofluorescence. Mono-cultured MOE:SCR cells were compared only to MOE:SCR cells in co-culture. All analyses excluded MOE:STING-OE cells. n≥3, analyzed by two-sided t-test. * $p < 0.05$, ** $p < 0.01$. Created in BioRender. Ventura, A. (2026) https://BioRender.com/3nm7dxd

(B) Representative images of mono-cultured MOE:SCR cells and MOE:SCR cells co-cultured with MOE:STING-OE cells treated with 500μM H_2O_2 for 6 hours and stained with DAPI (blue), γH2AX (green), and STING (yellow). STING-OE cells were identified by strong perinuclear STING staining (white arrow). γH2AX positive cells in MOE:SCR cells (perinuclear-STING negative) were quantified using imageJ analysis (right). Scale bar is 10um. n=4, analyzed by two-sided t-test. * $p < 0.05$

(C) MOE:GFP cells in mono-culture and in co-culture with STING-OE cells were incubated with 500μM H_2O_2 for 24 and 48 hours then apoptosis was measured by flow cytometry. Quantification of percent of cells undergoing apoptosis compares only MOE:GFP in both conditions. n=4

(D) Schematic depicting experimental design. Conditioned media was produced by challenging MOE:SCR and MOE:STING-OE cells treated with 500μM H_2O_2 for 24 hours. After filtration, conditioned media was incubated with MOE:SCR cells and re-spiked with 500μM H_2O_2. Created in BioRender. Ventura, A. (2026) https://BioRender.com/i8jazgi

(E) MOE:SCR cells were challenged with 500μM H_2O_2 in conditioned media from either MOE:SCR (SCR-CM) or MOE:STING-OE (SO-CM) and analyzed by immunoblot. n≥3

(F) qPCR analysis of *TNFa* expression in MOE:SCR and MOE:STING-OE cells after 6hr challenge with 500μM H_2O_2. n≥5, analyzed by one-way ANOVA followed by a Tukey's post-hoc. ** $p < 0.01$

(G) Representative images of colony forming efficiency of MOE:SCR cells treated with 500μM H_2O_2 +SCR-CM or SO-CM in combination with 1uM of neutralizing antibody against TNFα (TNFi) for 7 days. Colony number was quantified using ImageJ. n≥5, analyzed by one-way ANOVA followed by a Tukey's post-hoc. **** $p < 0.0001$

(H) Cellular viability of MOE:SCR and MOE:STING-OE cells treated with H_2O_2 + SCR-CM or SO-CM in combination with 1uM TNFi for 5 days. n≥3

(I) MOE:SCR cells were challenged with 500μM H_2O_2 in SCR-CM, SO-CM, or SO-CM +TNFi and analyzed by immunoblot.

(J) qPCR analysis of MOE:SCR cells treated with 500μM H_2O_2 in SCR-CM or SO-CM for 24 hours.

(K) WT organoids were treated with 250μM H_2O_2 in SCR-CM or SO-CM for 7 days. n≥5, analyzed by one-way ANOVA followed by a Tukey's post-hoc. ** $p < 0.01$, **** $p < 0.0001$

(L) STING−/− organoids were treated with 750μM H_2O_2 in SCR-CM or SO-CM for 7 days. n≥5, analyzed by one-way ANOVA followed by a Tukey's post-hoc. ** $p < 0.01$, **** $p < 0.0001$

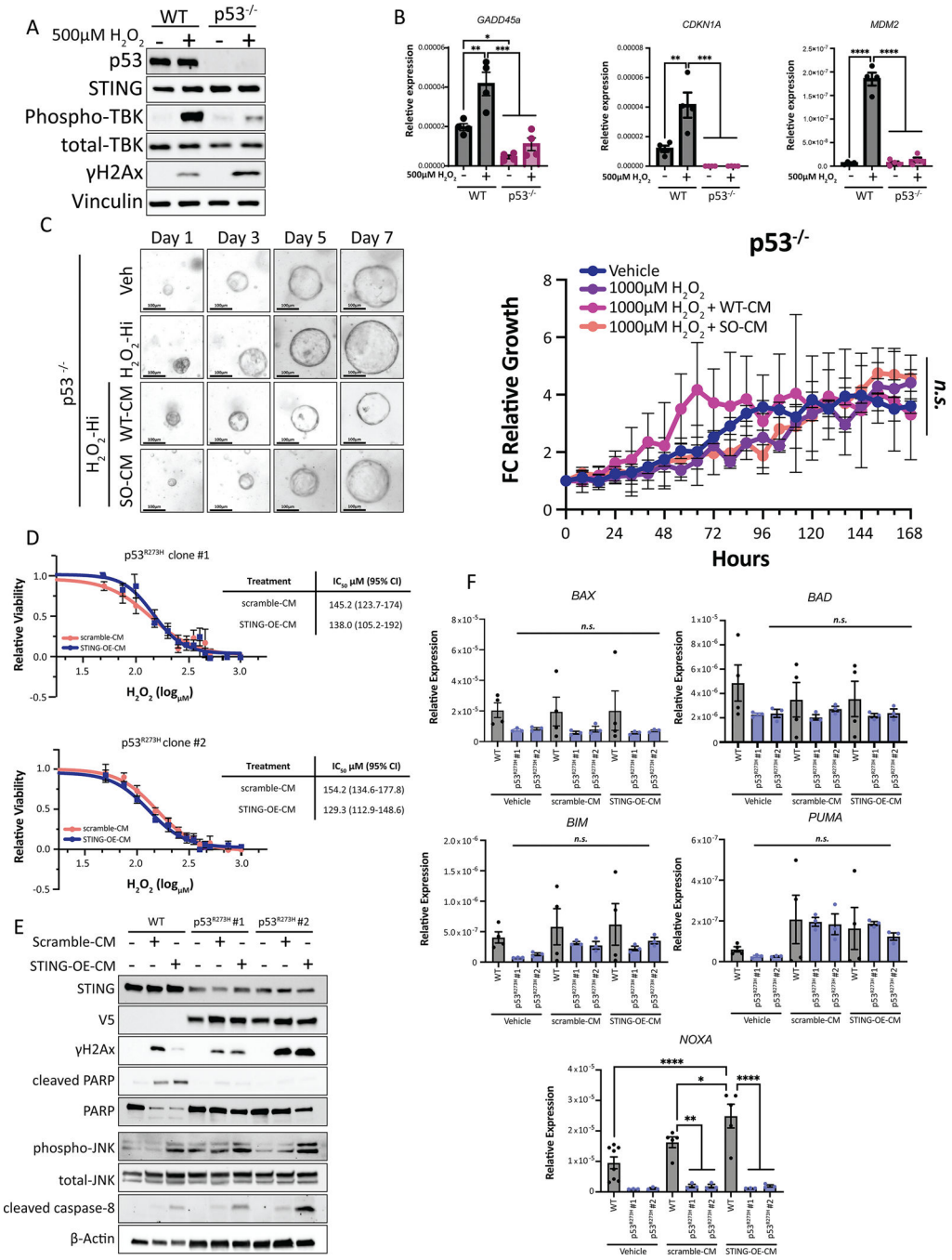

Figure 6. p53-Deficient Cells Evade Cell Death Triggered by Extrinsic STING Signaling

(A,B) Organoids from the oviducts of OVGP1-Cre-P53−/− mice were treated with tamoxifen (P53−/−) or vehicle control (WT). Organoids were then challenged with 500uM H_2O_2 and analyzed by (A) immunoblot and (B) qPCR. n≥4, analyzed by one-way ANOVA followed by a Tukey's post-hoc. * $p < 0.05$, ** $p < 0.01$, *** $p < 0.001$, **** $p < 0.0001$

(C) p53−/− organoids were treated with 750μM H_2O_2 in SCR-CM or SO-CM for 7 days and organoid growth was monitored by live cell imaging. n≥5, analyzed by one-way ANOVA followed by a Tukey's post-hoc. n.s. indicates no significant difference.

(D) MOE cells were virally transduced with v5-tagged mutant p53R270H (MOE:P53^{R270H} Clone1 and Clone2). Cellular viability of MOE:P53mut clones treated with w H_2O_2 + SCR-CM or SO-CM for 5 days was assessed by SRB assay. n≥3
(E,F) MOE: SCR and MOE:P53^{R270H} clones were treated with 500uM H_2O_2 H_2O_2 and analyzed by (F) immunoblot and (G) RNA qPCR analysis. n≥4, analyzed by one-way ANOVA followed by a Tukey's post-hoc. * $p < 0.05$, ** $p < 0.01$, *** $p < 0.001$, **** $p < 0.0001$